Supplement of Clim. Past, 20, 2117–2141, 2024
https://doi.org/10.5194/cp-20-2117-2024-supplement

Climate of the Past
Open Access
EGU

Supplement of

A continental reconstruction of hydroclimatic variability in South America during the past 2000 years

Mathurin A. Choblet et al.

Correspondence to: Mathurin A. Choblet (mathurin@choblet.com)

Supplement S1: Proxy record supplement

S1.1 Detailed spatiotemporal availability

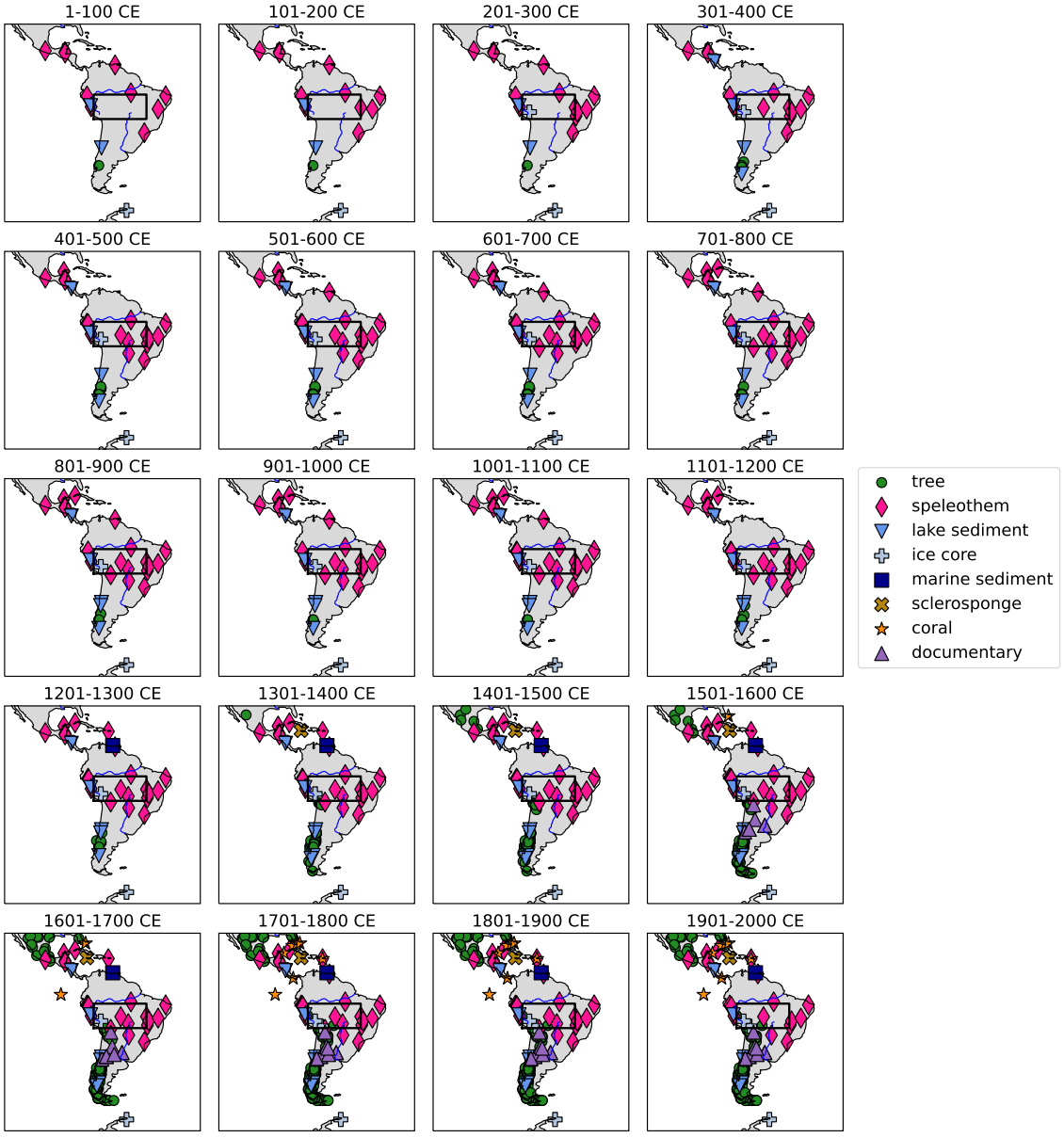

Figure S1.1. Spatiotemporal availability of the proxy records for each century . The black box represents the core region of the South American Summer Monsoon (Vuille et al., 2012)

S1.2 Proxy record lists

For an overview of all proxy records employed in this regional climate field reconstruction, the proxy records are grouped by climate archive type and presented in tabular form. In the *database* column, the proxy record databases from which the values were taken are named, in case the record is part of one. Additionally the original publications are cited in the *source* column. For the citations of proxy records that were part of a database, the reader is referred to the publications presenting the proxy record databases. The level of detail in the tables varies by climate archive type, as the information from column with unique entries (e.g. the proxy variable, PSM type, Seasonality or SNR) has been transferred to explanatory text above the tables to limit the size of the tables. All data processing steps can be retraced and reproduced with the Jupyter Notebooks accompanying this publication.

S1.2.1 Speleothems

The proxy variables are δ^{18}O of aragonite and δ^{18}O of calcite for all processed speleothem time series. For all speleothems, the same *precipitation weighting*-type PSM has been used, thus rendering the application of some additional seasonality restrictions unnecessary. The SNR is computed from the variance of the time series by assuming the same SNR for all speleothems (See Section S2.2). Whereas the speleothem time series have relatively high median temporal resolutions, all time series are resampled to 10 years resolution to conservatively account for smoothing effects in the karst.

For caves with multiple records of similar resolution, composites were computed according to Novello et al. (2021) (step 2 and 3 in section 3.3) by applying the following steps to the time series of various records in one cave during the overlap period 1) resampling all proxy time series to annual resolution, 2) standardizing the time series (zero-mean & standard deviation equal to one) 3) computing the mean of the overlapping values 4) destandardizing the mean time series using the mean and standard deviation of the time series which is longer. Further steps detailed in section 3.3 of Novello et al. (2021) are not applied, as these involve age model ensembles, which have not been used in this study. The practical computation of speleothem composites can be retraced in the Jupyter Notebooks accompanying this publication.

Nr	Site name	Location (Lat,Lon)	Time (CE)	Resolution time scale [yrs]	Database (ID in database)	Source	Comment
1	Dos Anas cave	22.4,276.0	746-2000	2	SISALv3 (443)	Fensterer et al. (2012)	
2	Tzabnah cave	20.7,270.3	487-2004	2	SISALv3 (147)	Medina-Elizalde et al. (2010)	
3	Perdida cave	18.0,293.0	1208-2003	2	SISALv3 (378)	Winter et al. (2011)	
4	Juxtlahuaca cave	17.4,260.8	0-2010	2	SISALv3 (286)	Lachniet et al. (2012)	
5	Macal Chasm	16.9,270.9	0-1992	3	SISALv3 (178)	Akers et al. (2016)	
6	Yok Balum cave	16.2,270.9	0-2005	1	SISALv3 (209)	Kennett et al. (2012)	Used longest record from location
7	Caripe Cave	10.2,296.4	0-1993	2	-	Medina et al. (2023)	
8	Paraiso cave	-4.1,304.6	0-1998	7	SISALv3 (424)	Wang et al. (2017)	
9	Trapiá cave	-5.6,322.3	0-1932	3	-	Utida et al. (2023)	
10	Shatuca cave	-5.7,282.1	0-1984	8	SISALv3 (434)	Bustamante et al. (2016)	
11	Palestina cave	-5.9,282.6	413-1850	5	SISALv3 (94)	Apaéstegui et al. (2014)	
12	Cascayunga Cave	-6.4,282.9	1088-1999	1	-	Bird et al. (2011b)	
13	Huagapo cave	-11.3,284.2	3-1993	2	SISALv3 (597,598)	Kanner et al. (2013)	Composite
14	Mata Virgem cave	-11.6,312.5	166-1814	1	-	Azevedo et al. (2019)	Used Mata Virgem 1 record
15	Cuíca cave	-11.7,299.4	338-2013	2	SISALv3 (752)	Libera et al. (2022)	
16	Diva cave	-12.4,318.4	2-1999	4	SISALv3 (113,146,203)	Novello et al. (2012)	Composite
17	São Matheus/Bernardo cave	-13.8,313.6	264-1998	1	SISALv3 (430,431)	Novello et al. (2018)	Composite
18	Pau d'Alho cave	-15.2,303.2	491-1860	1	SISALv3 (128)	Novello et al. (2016)	
19	Tamboril cave	-16.0,313.0	272-1982	2	SISALv3 (97)	Wortham et al. (2017)	
20	Umajalanta cave	-18.1,294.2	620-1863	2	SISALv3 (499,497,498,518)	Apaéstegui et al. (2018)	Composite
21	Jaraguá cave	-21.1,303.4	422-2000	3	SISALv3 (449)	Novello et al. (2018)	Composite as part of SISAL
22	Cristal Cave	-24.5,311.4	0-2006	2	-	Vuille et al. (2012)	

Table S1.1. Speleothem proxy records description table

S1.2.2 Lake sediment records

Only lake sediment records directly related to the isotopic composition of precipitation (and thus not mostly affected by additional evaporation) or already calibrated to temperature have been included. To make this distinction, the original publications have been consulted and records have been accordingly selected. This restriction excluded most lake sediment records available in the Iso2k database (Konecky et al., 2020). All lake sediment records are used on a time scale of five years, to account for the effect of bioturbation in the sedimentation process. For all lake sediments, the same SNR value has been assumed, also for temperature calibrated records which come with an error variance.

Nr	Site name	Location (Lat,Lon)	Time (CE)	Resolution	Proxy variable	PSM	Seasonality	Database (ID in database)	Source
1	Lago El Grancho	11.9,274.1	341-2004	4	δ^{18}O	prec. weighted	None	Iso2k (263)	Stansell et al. (2013)
2	Laguna Pumacocha	-10.7,283.9	0-2007	2	δ^{18}O	prec. weighted	None	Iso2k (343)	Bird et al. (2011a)
3	Laguna Chepical	-32.3,289.5	0-2005	1	tsurf	season	11,12,1,2	Pages2k (SAm_30)	de Jong et al. (2013)
4	Laguna Aculeo	-33.8,289.1	856-1997	1	tsurf	season	12,1,2	Pages2k (SAm_3)	von Gunten et al. (2009)
5	Laguna Escondida	-45.5,288.2	400-2008	1	tsurf	direct	None	Pages2k (SAm_31)	Elbert et al. (2013)
6	Lago Plomo	-47.0,287.1	1384-2001	1	tsurf	season	9,10,11,12,1,2	Elbert et al. (2015)	Elbert et al. (2015)
7	Lago Puyehue	-40.7,287.55	1408-1997	1	tsurf/spei	linear	-	Neukom and Gergis (2012)	Boës and Fagel (2008)

Table S1.2. Lake sediment proxy records description table

S1.2.3 Sclerosponge

For the conversion of the sclerosponge values from Montego Bay, Jamaica, to temperature, the formula presented in Haase-Schramm et al. (2003) was used. From the two provided records, we selected the record which was located closer the sea surface (see original publication for details). The time series values were resampled to five years to account for the non-annual resolution of the record.

Nr	Site name	Location (Lat,Lon)	Time (CE)	Resolution	Proxy variable	PSM	Seasonality	SNR	Database (ID in database)	Source
1	Montego Bay, Jamaica	18.5,282.0	1356-1991	5	tsurf	direct	None	assumed	Pages2k (150)	Haase-Schramm et al. (2003)

Table S1.3. Sclerosponge proxy record description table

S1.2.4 Marine sediment

The Cariaco Basin record from Black et al. (2007) was the only marine sediment included in our regional climate field reconstruction, as other marine sediment from South and Central America only provide a longer than decadal resolution. Due to the exceptionally high sedimentation rate in the Cariaco Basin, the record was treated as an annual record according to its temporal resolution.

Nr	Site name	Location (Lat,Lon)	Time (CE)	Resolution	Proxy variable	PSM	Seasonality	SNR	Database (ID in database)	Source
1	Cariaco Basin	10.8,295.2	1221-1990	1	tsurf	season	3,4,5	assumed	Pages2k (11)	Black et al. (2007)

Table S1.4. Marine sediment proxy record description table

S1.2.5 Ice cores

For all ice core δ^{18}O record locations, the precipitation weighting PSM has been applied, rendering the definition of a seasonality unnecessary. For all ice core proxy records, an SNR value was assumed to compute the error variance.

Nr	Site name	Location (Lat,Lon)	Time (CE)	Proxy variable	Database (ID in database)	Source	Comment
1	Quelccaya Ice Cap	-13.9,289.2	226-2009	δ^{18}O	Pages2k (SAm_026)	Thompson et al. (2013)	
2	Illimani	-16.6,292.2	1771-1998	D	Iso2k (485)	Hoffmann et al. (2003)	Deuterium converted to δ^{18}O with factor 1/8
3	James Ross Island	-64.2,302.3	0-2007	D	Pages2k (Ant_10)	Abram et al. (2013)	Deuterium converted to δ^{18}O with factor 1/8

Table S1.5. Ice core proxy records description table

S1.2.6 Corals

All coral proxy records were used on an annual time scale. For the PSM, the linear PSM for temperature was used, thus all records were calibrated to temperature. Calibration values (including SNR estimates) were calculated for the annual and seasonal reconstruction/calibration separately.

Nr	Site name	Location (Lat,Lon)	Time (CE)	Resolution	Proxy variable	SNR (Ann.,DJF)	Database (ID in database)	Source
1	Gingerbread Bahamas	25.8,281.4	1552-1991	1	calcification	0.2, 0.15	PAGES2K-Ocn_065	Saenger et al. (2009)
2	Alinas Reef, Biscayne National Park, Florida	25.4,279.8	1751-1986	1	δ^{18}O	0.1,0.13	Iso2K-255	Swart et al. (1996)
3	Dry Tortugas	24.6,277.7	1733-2008	1	Sr_Ca	0.55,0.97	PAGES2K-Ocn_070	DeLong et al. (2014)
4	Punta Maroma, Mexico	20.8,273.3	1773-2009	1	calcification	0.88,0.4	PAGES2K-Ocn_073	Tierney et al. (2015)
5	Turrumote Reef, Puerto Rico	17.9,293.0	1751-2004	1	δ^{18}O	0.73,0.59	PAGES2K-Ocn_111	Kilbourne et al. (2008)
6	Secas Island, Panama	8.0,278.0	1707-1984	1	δ^{18}O	0.27,0.23	PAGES2K-Ocn_104	Linsley et al. (1994)
7	Urvina Bay	-0.4,268.8	1607-1981	1	δ^{18}O	0.61,0.34	PAGES2K-Ocn_087	Dunbar et al. (1994)

Table S1.6. Coral proxy records description table

S1.2.7 Documentary records

All employed documentary indices were taken from the NOAA database (https://www.ncei.noaa.gov/access/paleo-search/study/8703) and were presented in Neukom et al. (2009). No seasonality restriction was imposed for using the data as the calibration to instrumental variables for the linear PSM was computed for the annual and summer season separately. All documentary records were used on an annual time scale.

Nr	Site name	Proxy variable	Location (Lat,Lon)	Time (CE)	SNR (Ann.,DJF)	Database	Source
1	Potosi	precipitation index	-19.6,294.3	1585-2005	0.32, 0.22	NOAA	Neukom et al. (2009)
2	Dulce	river runoff index	-27.0,295.0	1750-1977	0.27,0.29	NOAA	Neukom et al. (2009)
3	Tucuman	precipitation index	-27.0,295.0	1548-2005	0.65,0.36	NOAA	Neukom et al. (2009)
4	Santiago del Estero	precipitation index	-27.8,195.7	1750-2005	0.47,0.38	NOAA	Neukom et al. (2009)
5	Santa Fe and Corrientes	precipitation index	-30.0,300.0	1590-2006	0.73,0.59	NOAA	Neukom et al. (2009)
6	Mendoza	river runoff index	-32.0,292.0	1599-2000	0.27,0.21	NOAA	Neukom et al. (2009)
7	Mendoza	precipitation index	-32.0,292.0	1600-1985	0.42,0.34	NOAA	Neukom et al. (2009)
8	Central Andes	snow depth index	-33.0,290.0	1760-1996	0.64,0.54	NOAA	Neukom et al. (2009)
9	Santiago de Chile	precipitation index	-33.3,289.7	1540-2006	0.49,0.45	NOAA	Neukom et al. (2009)
10	Parana	river runoff index	-30.0,300.0	1590-1993	0.3,0.33	NOAA	Neukom et al. (2009)
11	Cordoba	precipitation index	-31.0,296.0	1700-2005	0.42,0.27	NOAA	Neukom et al. (2009)

Table S1.7. Documentary records description table

S1.2.8 Trees

The employed tree records are described solely in text form rather than tabular format due to their large quantity. The proxy data from trees was mainly taken from three proxy record databases according to the selection criteria outlined in the main text. This selection resulted in 203 tree proxy time series from the South American Drought Atlas (Morales et al., 2020), 42 from Breitenmoser et al. (2014), as used in and published alongside Steiger et al. (2014), and 5 records from the Pages2k database (Emile-Geay et al., 2017). We checked for potential overlaps between these proxy databases and excluded double/triple records. As the SADA database only extends back to 1400CE, six records from it have been replaced by the longer original record data which are available in the NOAA database (see code of this publication for exact documentation). All these data bases use tree ring width as a proxy from trees, and not Maximum Wood Density (MXD). In addition to these tree ring data sources, we used four single records/tree ring composites , namely from the central Altiplano (Morales et al., 2012), the northern altiplano (Morales et al., 2023), the western Amazon (Humanes-Fuente et al., 2020) and near the Perito Moreno glacier in Patagonia (Grießinger et al., 2018). For this last tree proxy record, the proxy variable is δ^{18}O in wood and not tree ring width, but this record has also been calibrated to instrumental variables as all other tree ring records, because precipitation δ^{18}O can not be directly related to δ^{18}O in wood. No seasonality restriction was imposed for using the data as the calibration to instrumental variables for the linear PSM was computed for the annual and summer season separately. All used tree records have annual resolution.

Supplement S2: Methodology

S2.1 Algorithm sketches

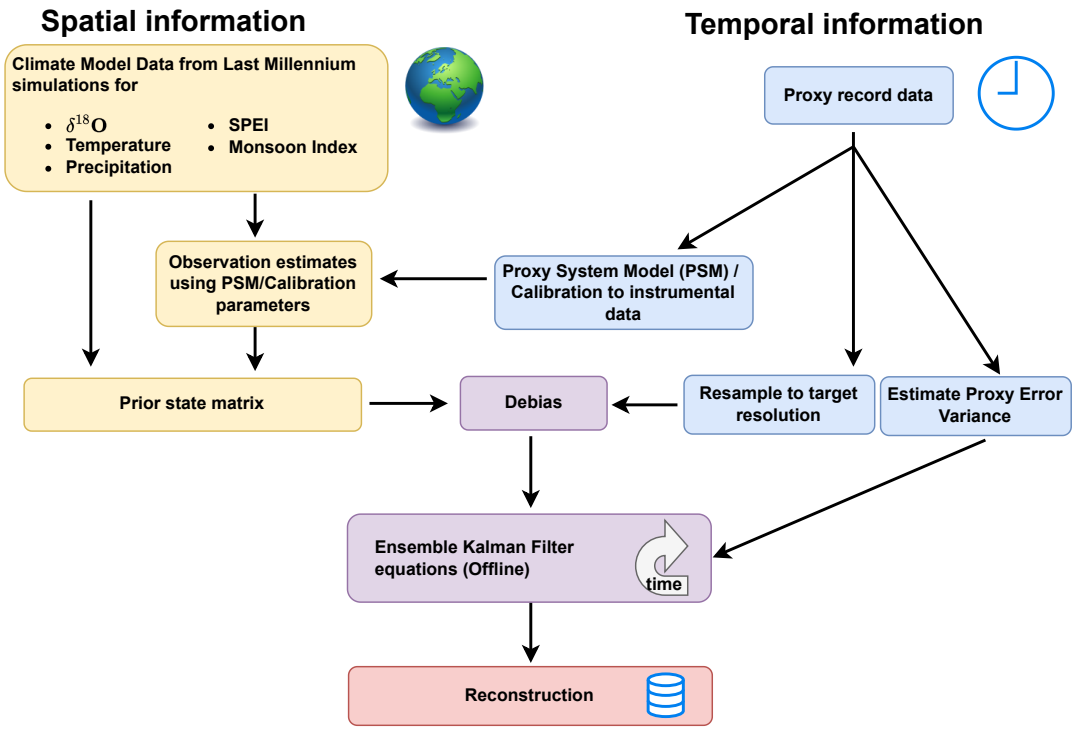

Figure S2.1. Algorithm sketch for multi-timescale Paleoclimate Data Assimilation Algorithm. See main text for a description of the individual steps.

$$\mathbf{X}^f = \begin{pmatrix} \mathbf{X}_{120} \\ \mathbf{X}_{50} \\ \dots \\ \mathbf{X}_{930} \end{pmatrix} \Rightarrow \overbrace{\begin{pmatrix} \mathbf{X}_{120} & \mathbf{X}_{121} & \dots & \mathbf{X}_{129} \\ \mathbf{X}_{50} & \mathbf{X}_{51} & \dots & \mathbf{X}_{59} \\ \dots & \dots & \dots & \dots \\ \mathbf{X}_{930} & \mathbf{X}_{931} & \dots & \mathbf{X}_{939} \end{pmatrix}}^{\text{block size=10 years}} \Big\} N_y \text{ ensemble members}$$

Figure S2.2. Illustration of how single-time scale PaleoDA prior, consisting of a random collection of climate fields, is extended into a matrix which also contains the subsequent years for multi-time scale PaleoDA. Each $\mathbf{X}_i$ corresponds to the mean climate field of one simulation year, the index denotes the year of the simulation that was randomly selected for creating the ensemble. The $\mathbf{X}_i$ could also be depicted explicitly as a vector, thus rendering the matrix three-dimensional. In the multi-time scale PaleoDA, rows of the matrix are averaged over several years in order to assimilate multiyear means.

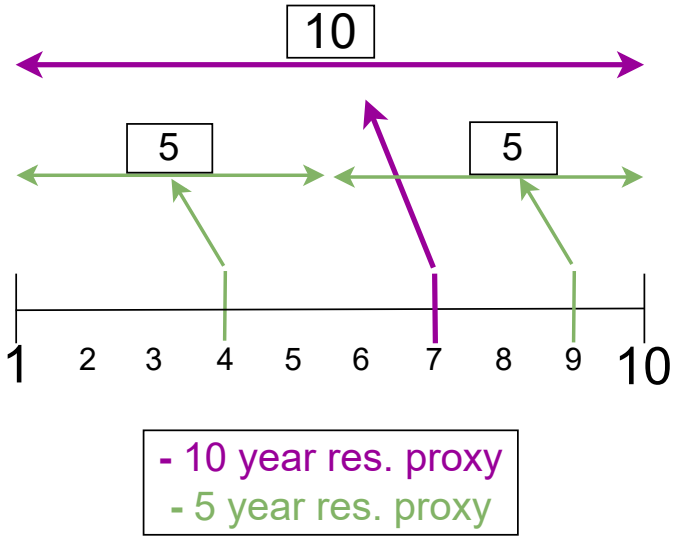

Figure S2.3. Assignment of non-annually resolved proxy records to 5 and 10 year time scales (e.g. lake records and speleothems in our reconstruction). During the multi-time scale PaleoDA, the values of these types of proxies are assigned to the 5 or 10 year block means (see Figure Figure S2.2 instead of annual values. To facilitate the assignment to the blocks, the non-annually resolved proxy records are resampled to 5 and 10 year resolutions as described in the main text.

S2.2 Observation error estimation from the Signal-to-Noise Ratio (SNR)

We estimate the observation error variance $\mathbf{R}$ (Equation 2) for each proxy record from an assumed signal-to-noise ratio (SNR).

The SNR is defined as the ratio of the standard deviations of the unperturbed time series T and the white noise N:

$$\text{SNR} := \frac{\text{std}(T)}{\text{std}(N)} \tag{S2.1}$$

As the observation error variance $\mathbf{R}$ is by definition equal to the squared standard deviation of the noise N, we get for $\mathbf{R}$

$$\mathbf{R} = \text{std}(N)^2 = \text{var}(N) \tag{S2.2}$$

$$\Rightarrow SNR = \frac{\text{std}(T)}{\sqrt{\mathbf{R}}} \tag{S2.3}$$

$$\Rightarrow \mathbf{R} = \frac{\text{var}(T)}{\text{SNR}^2} \tag{S2.4}$$

The variance of T is not known directly because the proxy record time series Y represents the noisy time series $T + N$, whose variance can be used to compute $\text{var}(T)$. When assuming that N and T are uncorrelated, their variances are additive.

$$\text{std}(T+N) = \sqrt{\text{var}(T+N)} \tag{S2.5}$$

$$= \sqrt{\text{var}(T) + \text{var}(N) + \text{cov}(T,N)} = \sqrt{\text{var}(T) + \text{var}(N)} \tag{S2.6}$$

$$= \sqrt{\text{var}(T) + \mathbf{R}} \tag{S2.7}$$

$$\Rightarrow \text{var}(T) = \text{var}(T+N) - \mathbf{R} \tag{S2.8}$$

Using the relationship from equation S2.8 in equation S2.4 we get

$$\mathbf{R} = \frac{\text{var}(T+N) - \mathbf{R}}{SNR^2} \tag{S2.9}$$

$$\Rightarrow \mathbf{R} = \frac{\text{var}(T+N)}{1+SNR^2} = \frac{\text{var}(Y)}{1+SNR^2} \tag{S2.10}$$

Using equation S2.10, the observation error $\mathbf{R}$ can be estimated from the variance of the proxy record time series and by assuming a specific SNR value for the proxy records, which does not need to be the same for all proxy records.

Supplement S3: Validation of reconstruction

S3.1 Spatial reconstruction skill using gridded instrumental data

To evaluate the spatial reconstruction skill of our reconstructions, we compare these to gridded instrumental datasets, Berkeley Earth (Rohde and Hausfather, 2020) for temperature and CRUTS 4 (Harris et al., 2020) for precipitation. A reference SPEI dataset is computed from CRUTS 4 using Thornthwaite's method for estimating potential evapotranspiration. The validation periods are 1920 - 2000 CE for temperature and 1950 - 2000 CE for precipitation and the SPEI, due to limited local instrumental, radiosonde and satellite precipitation data during the first half of the 20th century. Until the second half of the 20th century, South America lacked extensive weather station coverage, with only a few stations mainly situated in coastal regions and the Southern part of the continent (See Figure 1 in Harris et al., 2020). Estimates of precipitation, which is a more localized phenomenon than temperature, are particularly affected by this limited station coverage. Precipitation estimates are considered more reliable since the deployment of the global radiosonde network in 1958 and satellite-derived rainfall estimates from the late 1970s (Garreaud et al., 2009). Consequently, the time period suitable for meaningful calibrations/validations using instrumental precipitation data is usually restricted to the second half of the 20th century (e.g. Morales et al., 2020). The validation period is, thus, the same as the calibration period of the tree rings and corals, which can be considered problematic. Unlike other climate field reconstruction techniques such as PCR (e.g. Neukom et al., 2010, 2011), PaleoDA with linear statistical PSMs does not strictly require the separation of calibration/validation data for two reasons. Firstly, the statistical PSM estimates regression parameters using local observational data, which are then applied to independent model simulation data. The model simulation data's mean and spatial covariances are not debiased with respect to the observational data, and thus importantly influence the reconstruction. In contrast, techniques like Point by Point regression (e.g. Morales et al., 2020) estimate a linear regression model for each reconstructed grid cell, resulting in more instrumentally tuned reconstructions. Secondly, the calibration process predicts proxy records from instrumental data, while the validation process predicts instrumental data from proxy records. This non-symmetry introduces information loss. Additionally, using multiple variables as predictors simultaneously in the reconstruction can potentially introduce errors through inadequate covariances in the prior.

As skill metrics, we choose the widely employed Pearson correlation and the Continuous Ranked Probability Skill Score (CRPSS) (Wilks, 2011). The correlation is a simple similarity metric with range $[-1, 1]$, which rewards a correct phasing of the reconstructed signal with respect to the observational data. In the correlation plots, we further denote significant correlations according to an effective p-value < 0.05. The effective p-value takes into account the smaller number of degrees of freedom in autocorrelated time series (Bretherton et al., 1999). Note, that, in a strict sense, correlations require detrended time series. We choose to not detrend the time series to also evaluate the skill of the reconstruction to capture trends, similar to previous PaleoDA reconstructions (e.g. Tardif et al., 2019; Steiger et al., 2018) In contrast, the CRPSS is considered a strictly proper scoring metric (Gneiting and Raftery, 2007) because it takes into account the posterior reconstruction distribution instead of the ensemble mean. We assume Gaussian statistics and, thus, characterize it via the ensemble mean and standard deviation. The CRPSS is the skill score version of the Continuous Ranked Probability Score (CRPS) and is computed as 1-CRPS_{rec}/CRPS_{ref}, where CRPS_{ref} is the CRPS value for a reference distribution. CRPS rewards small biases, correct variances and ensemble spread. For the reference CRPS score, we take the ensemble statistics of the uninformed prior ensemble as in Steiger et al. (2018). The CRPSS values lie in the range $(-\infty,1]$, where positive values denote reconstructions more skillful than the prior. As the CRPSS values are computed for each validation time step, we compute the temporal mean of these values and denote them as CRPSS. Both metrics do not take observational uncertainties into account. For all skill scores, we have initially also considered applying a low-pass filter to the time series before applying the skill metrics, as we estimate our reconstruction to be more meaningful on longer than annual time scales. However, we have finally refrained from this idea as the validation period is pretty short (80 and 50 years) and for correlation, higher absolute correlations and effective p-values are expected due to the filtering introducing auto-correlation.

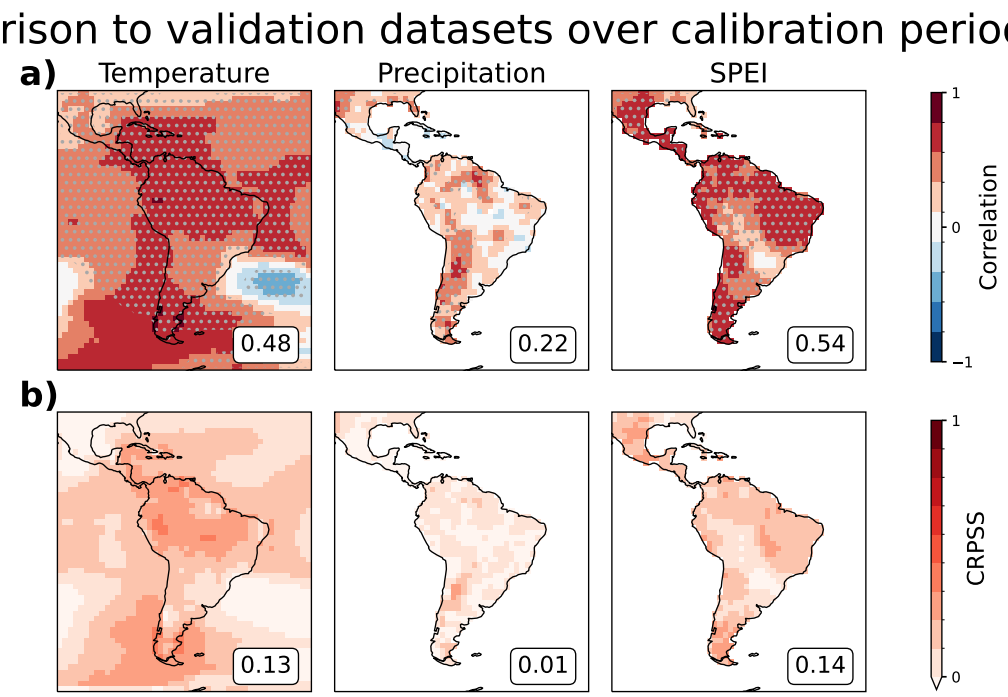

Figure S3.1. Comparison to validation data sets over calibration period: validation skill metrics from comparing our reconstruction to the Berkeley Earth surface temperature dataset (Rohde and Hausfather, 2020) for the years 1920 - 2000 CE, the CRUTS 4 precipitation dataset (Harris et al., 2020) for the years 1950 - 2000 CE and SPEI calculated using temperature and precipitation from the CRUTS 4 dataset for the years 1950 - 2000 CE. Precipitation skill is only evaluated on land as the instrumental dataset only provides precipitation over land. The panels in a) show the correlation with stippling indicating effective p-values smaller than 0.05. The panels in b) show the results for the CRPSS. The values in the lower right corner denote the mean skill score. See text for details. The spatial reconstruction skill for the reconstruction of austral summer (DJF) is displayed in Figure Figure S3.2.

Figure Figure S3.1 shows the skill metric results for the annual reconstruction. Significant positive correlations are found for almost all terrestrial locations in the surface temperature and SPEI reconstruction (mean values 0.48 and 0.54). Due to the increasing temperature trend of the current warm period (CWP), such high correlations can be expected, also for SPEI, which depends on temperature via evapotranspiration. For precipitation positive significant correlations are mainly found in the Andes and parts of northern and eastern South America (mean value 0.22). We find the highest similarities close to the proxy record locations, in particular the Andes, which reflects the local character of precipitation changes and the lack of a clear trend in precipitation during the 20th century. CRPSS values for temperature and SPEI are mostly positive (mean 0.13 and 0.14), whereas for precipitation positive values stay close to zero (mean 0.01).

The skill metric values for the austral summer reconstruction (DJF) are shown in Figure Figure S3.2. The values are consistently lower than for the annual means, with the highest similarity encountered for the Southern Cone. We suppose, that despite calibrating the tree rings and corals to austral summer means, their proxy record locations are less representative for the whole continent compared to annual means. In the presentation of the results, we thus focus on the annual reconstruction.

Note, that this type of 20th century validation mainly reflects the skill of reconstructing the continent's hydroclimate through tree proxy data, the most abundant annually dated climate archive in our database during the instrumental era. The speleothems, which are a key archive for reconstructing the entire past two millennia, are only used on a decadal time scale and thus only contribute very little to reconstructions during the 20th century. Moreover, the focus on our data analysis will lie on decadal to centennial climate changes. The instrumental record is too short to validate the reconstructions skill on these time scales.

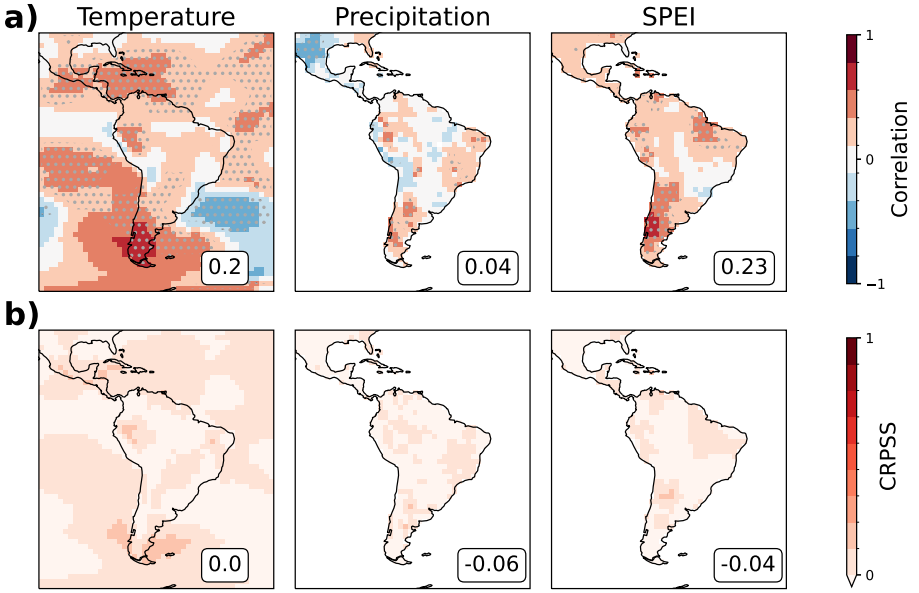

Figure S3.2. Validation skill metrics from comparing our austral summer (DJF) reconstruction to instrumental data. See caption of Figure Figure S3.1 for details.

Finally, it needs to be accounted that in most climate field reconstructions, the number of proxy records available in the validation/calibration period is usually order of magnitudes larger than in the preceding centuries. Hence, the obtained skill is not necessarily representative for the rest of the reconstruction period.

S3.2 Precipitation in the core monsoon region

A central aspect of this study consists of reconstructing the variability of the SASM according to the definition of Vuille et al. (2012), who proposed computing the mean precipitation in the core monsoon region (5°S–17.5°S/72.5°W–47.5°W, see black rectangle in Figure 1) as an indicator of monsoon strength. The SASM reaches its peak intensity during the austral summer months (DJF). Nevertheless, we focus on annual mean precipitation values in the core monsoon region for the validation, as we consider our annual reconstruction to be more reliable (see Section S3.1). Figure Figure S3.4 shows the reconstructed mean precipitation anomaly in the core monsoon region compared to the values computed from the instrumental datasets CRUTS 4 (Harris et al., 2020) and GPCC (Schneider et al., 2008).

One important uncertainty in this type of validation is the inconsistency of different precipitation validation datasets, which is even more apparent when including the data from the 20CR reanalysis project (Compo et al., 2011)(Figure S3.5). Computing the pointwise correlation between the datasets for the annual mean precipitation values (Figure S3.3 highlights, that in the core monsoon region, the low density of meteorological stations also discussed in Section S3.1 leads to lower similarity compared to the rest of the continent.

It is apparent that our reconstruction does not capture short-term precipitation fluctuations and clearly underestimates precipitation variability for the short instrumental period, as it stays in the range of [-5,5] mm/month, whereas the instrumental data fluctuates in the range [-20,20] mm/month. The intensity of these fluctuations also shows considerable disagreement between the two instrumental datasets during the first half of the 20th century.

Table S3.1 presents the skill scores for the reconstructed monsoon index depending on whether all proxy records, only tree data, or all proxy records without the tree data is used. These scores have been computed for the calibration period, but

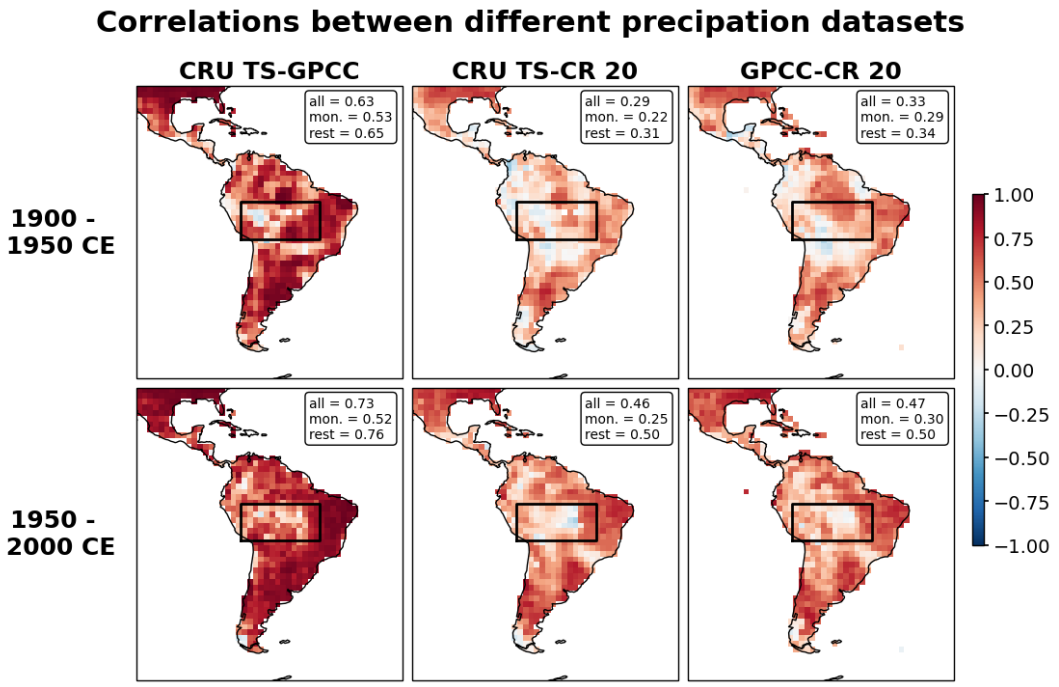

Figure S3.3. Correlation of annual mean precipitation values in the CRU (Harris et al., 2020), GPCC (Schneider et al., 2008) and 20CR (Compo et al., 2011) datasets. The correlation is computed separately for the period 1900-1950 CE, prior to the onset of radiosonde precipitation monitoring (1958), and for the second half of the 20th century. The inset box computes the average correlation for all grid cells (all), for the core monsoon region (mon.) and for all grid cells except the core monsoon region (rest).

also the entire 20th century. Overall, the skill scores are low and inconclusive. In contrast to what one would expect, the tree data, which is calibrated to instrumental temperature, precipitation, and SPEI data, yields the lowest skill scores. The tree data, which is mainly located in the central and southern Andes and thus outside the core monsoon region does not seem to be a good predictor for mean precipitation changes in the core monsoon region. This emphasizes the need to add precipitation sensitive proxies within, or at least closer to the core monsoon region. In our study, additional value is gained through the inclusion of speleothem records, but which are not highly resolved enough for a validation during the short instrumental period. This assessment emphasizes that the reconstructed precipitation changes likely do not accurately capture short-term variations in precipitation. We assume that the recorded changes are more likely to reflect long-term trends, which cannot be adequately validated due to the limited duration of instrumental data. Due to its limitations and despite its frequent use in PaleoDA, the instrumental validation exercise is thus not a proper tool for our reconstruction.

S3.3 Drought Index validation for the Southern Cone

A reference reconstruction of dry and wet conditions for Southern South America in the period 1400 - 2000 CE is the South American Drought Atlas (SADA) (Morales et al., 2020), whose input tree ring data is also partially employed our study. The SADA reconstructs the self-calibrated PDSI (scPDSI) using Point-by-Point Regression, a climate field reconstruction technique that is more calibrated towards local instrumental data. The SADA can be considered the most elaborate drought index reconstruction for the region. Although our reconstruction does not include scPDSI as a reconstructed variable, we compute the correlation to our reconstructed SPEI drought index to assess their similarity (Figure Figure S3.4). Despite scPDSI and PDSI capturing different types of droughts, we expect similarity in the phasing of drier and wetter periods due to using similar input data. Additionally, the reconstructed SPEI is compared to the SPEI from the PHYDA reconstruction (Steiger

		1950 - 2000 CE		1901 - 2000 CE	
		CRUTS 4	GPCC	CRUTS 4	GPCC
All proxy records	Corr	0.18	0.07	0.1	0.03
	CRPSS	-0.01	-0.02	-0.03	-0.03
Only trees	Corr	-0.06	-0.14	-0.10	-0.08
	CRPSS	-0.07	-0.06	-0.09	-0.05
No trees	Corr	0.20	0.11	0.18	0.08
	CRPSS	-0.04	-0.03	-0.05	-0.03

Table S3.1. Skill scores for the annual reconstruction of precipitation in the core monsoon region of the SASM during the 20th century with respect to CRUTS 4 (Harris et al., 2020) and GPCC (Schneider et al., 2008). For the experiments of the first row, all proxy records have been used, in the second row only tree data has been employed and in the third row the tree data has been explicitly excluded. The correlation values are presented without effective p-values, as none was significant ($\alpha < 0.05$).

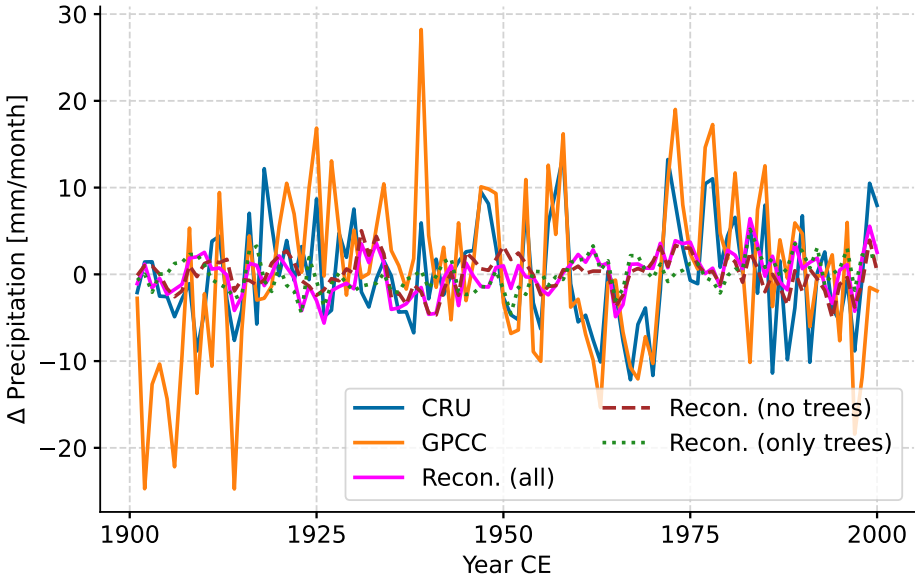

Figure S3.4. Annual precipitation anomaly in the core monsoon region ($5° - 17.5°$ S / $72.5° - 47.5°$ W) for the years 1901 - 2000 CE in the CRUTS 4 and GPCC datasets and our reconstruction (including all proxy records). For all time series the mean of the period 1901 - 2000 CE was subtracted.

et al., 2018), which also employs PaleoDA as a reconstruction technique using a subset of the SADA tree data. In PHYDA, where both SPEI and PDSI are reconstructed, both indices are highly correlated (not shown), we thus consider that in PHYDA both indices can be used interchangeably.

The largest similarity in terms of significant positive correlation for our reconstruction and SADA can be found close to the tree data locations in the Andes, especially Patagonia. The lowest similarity is found in the Pampas and the La Plata basin. Comparing the similarity of our reconstruction to SADA to the similarity of SADA and PHYDA, we find higher mean correlations than for PHYDA (0.12 vs 0.07 for the period 1400-1900 CE and 0.16 vs 0.12 for the period 1901-2000 CE). The correlations between our reconstruction and PHYDA are higher and spatially extensive for the entire Southern Cone (0.22 and 0.42), except for southern Patagonia. This reflects that both employ the same reconstruction technique, and in part the same proxy and model data, as PHYDA is based on the CESM model, whose isotope-enabled version is also part of our multi-model ensemble.

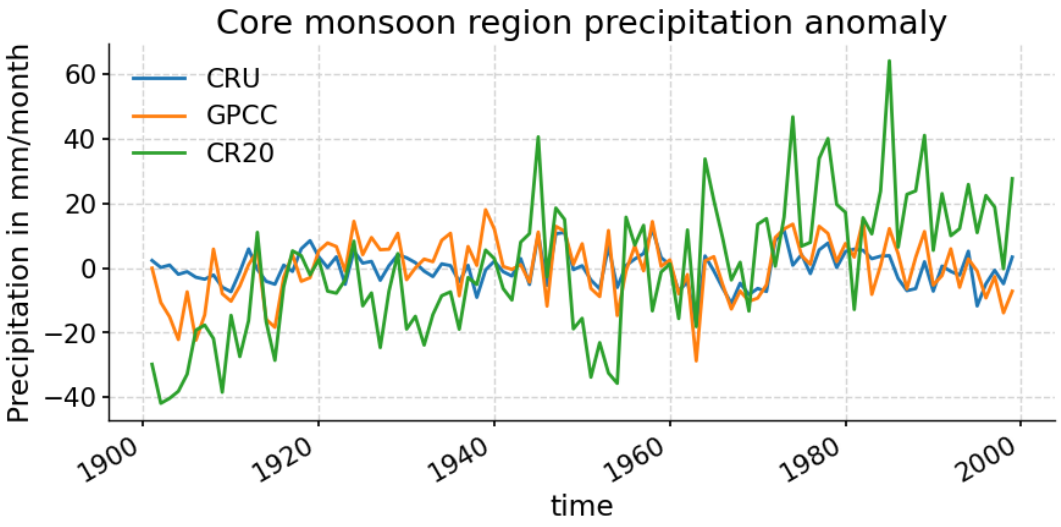

Figure S3.5. Annual core monsoon region precipitation anomaly from CRU (Harris et al., 2020), GPCC (Schneider et al., 2008) and 20CR (Compo et al., 2011)

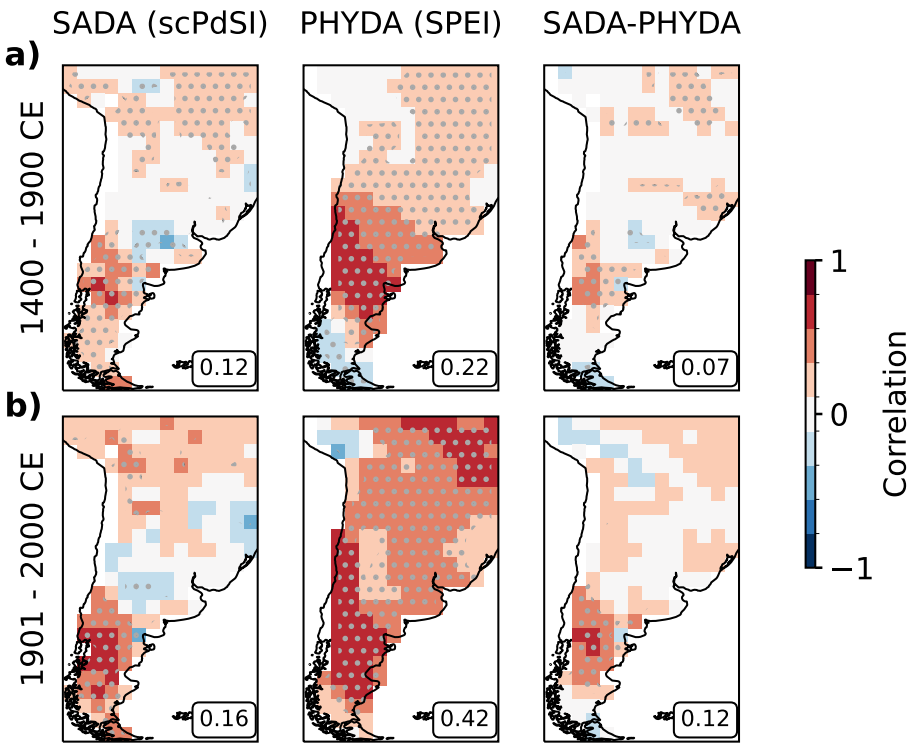

Figure S3.6. Evaluation of correlation of the reconstructed annual SPEI to scPDSI from the SADA (Morales et al., 2020) and SPEI from the PHYDA (Steiger et al., 2018) (left and center panels). The right panel compares the correlation of scPDSI in SADA and PDSI in PHYDA. Grid cells with effective p-values <0.05 are indicated by stippling. The upper row (a) shows the correlation for the period 1400 - 1900 CE and the lower row (b) for the period 1901 - 2000 CE. The SADA and PHYDA datasets have been regridded to the spatial resolution of our reconstruction.

Supplement S4: Additional Result Figures

Mean anomaly fields (Figure 3) for austral summer reconstruction

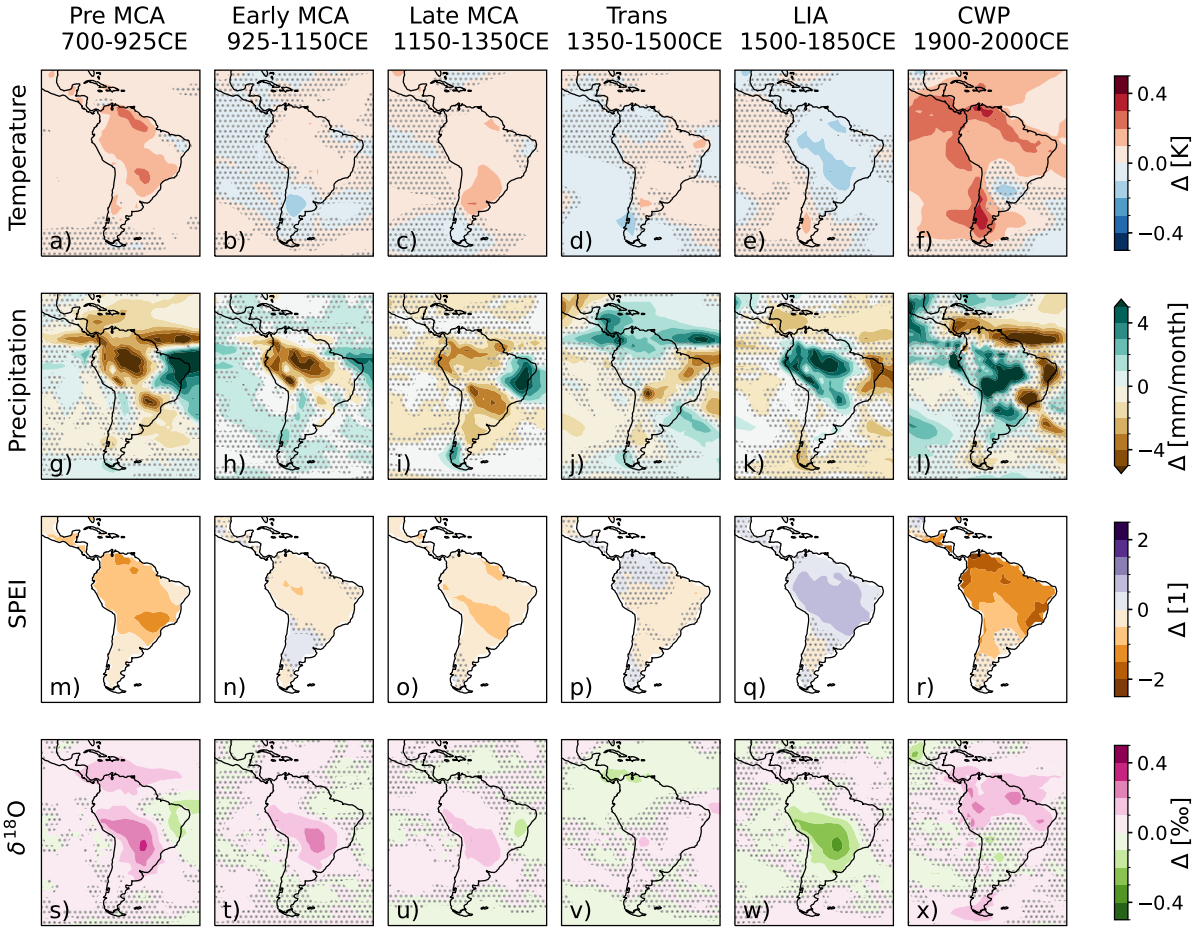

Figure S4.1. Same as Figure 3 for the austral summer (DJF) reconstruction. Stippling indicates grid cells where the difference to the Last Millennium values is not significant according to a Welch's t-test ($\alpha > 0.01$).

Mean anomaly fields (Figure 3) for reconstruction with different proxy error definition

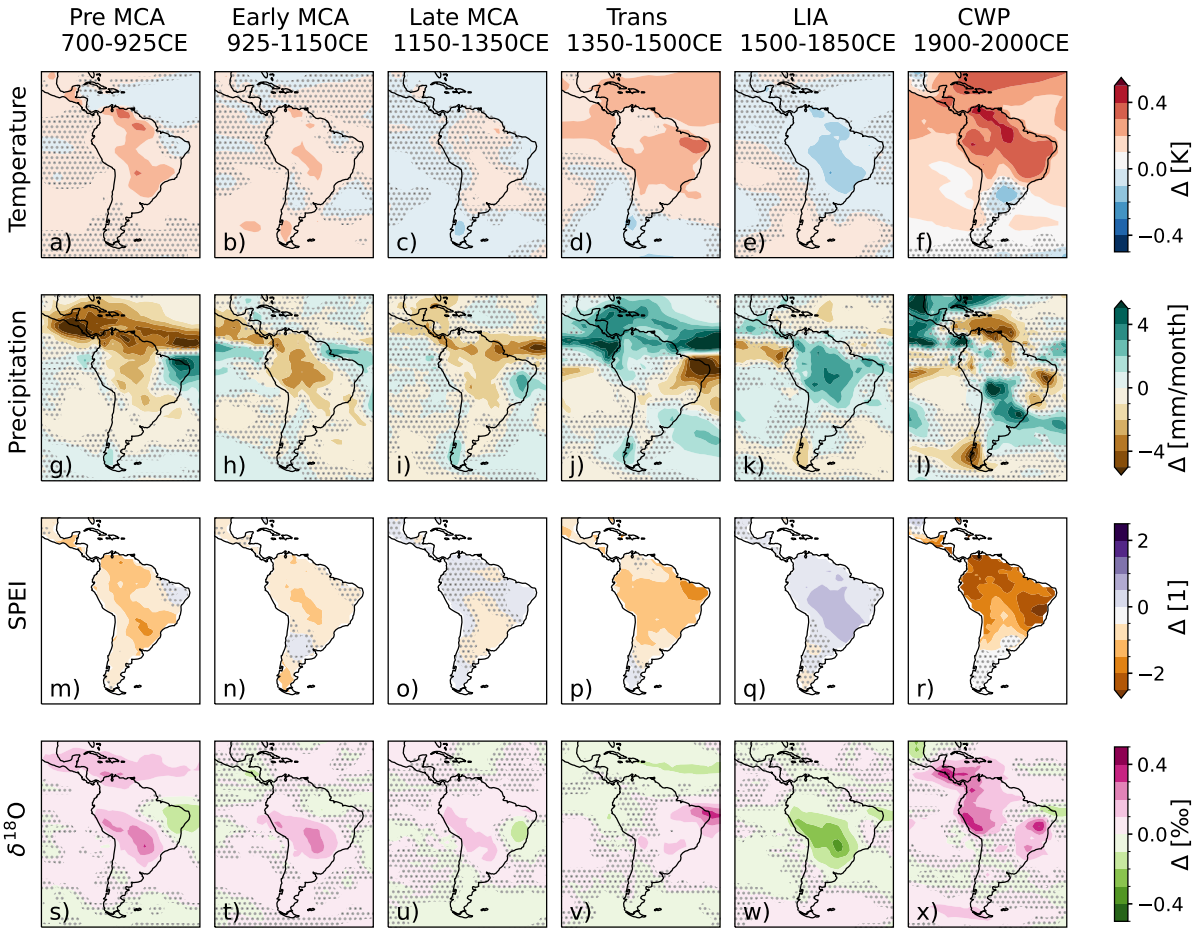

Figure S4.2. Same as Figure 3 applying a proxy error variance equal to the prior variance instead of the SNR=0.5 proxy error definition. Stippling indicates grid cells where the difference to the Last Millennium values is not significant according to a Welch's t-test ($\alpha > 0.01$).

205 **Mean anomaly fields (Figure 3) for reconstruction only using speleothem proxy records**

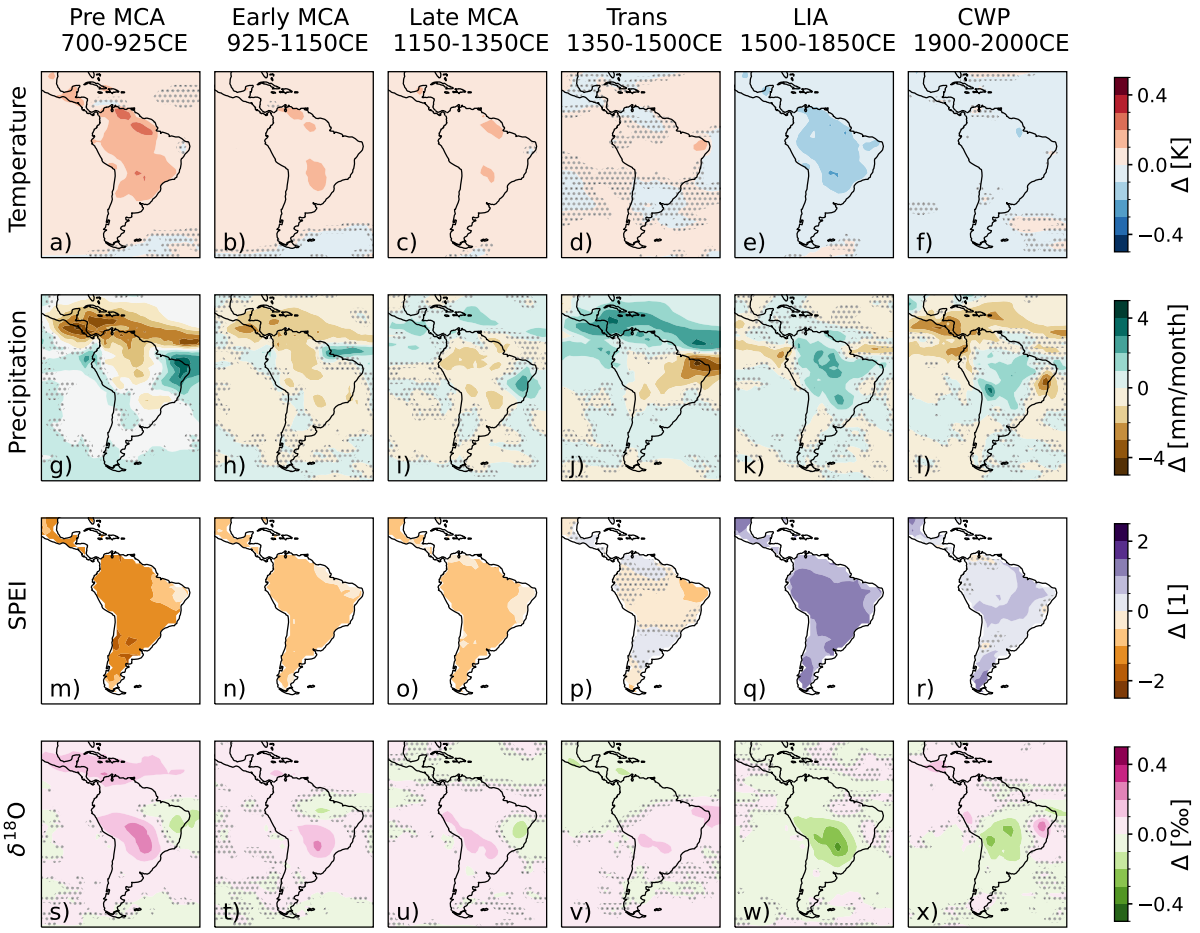

Figure S4.3. Same as Figure 3 but for the reconstruction that only uses speleothems as proxy record input data. Stippling indicates grid cells where the difference to the Last Millennium values is not significant according to a Welch's t-test ($\alpha > 0.01$).

Mean anomaly fields (Figure 3) for reconstruction excluding speleothem proxy records

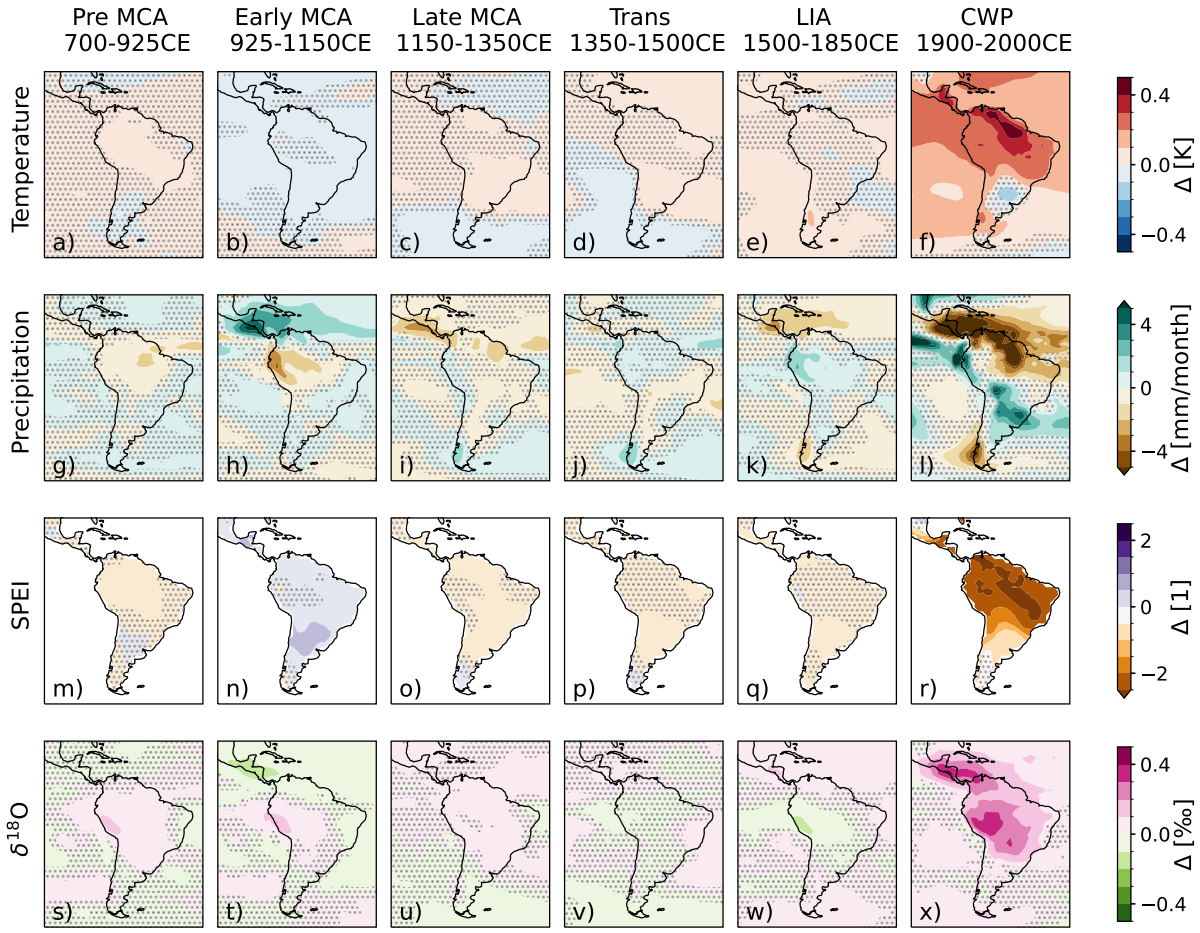

Figure S4.4. Same as Figure 3 but for the reconstruction that uses all proxy records except the speleothems as proxy record input data. Stippling indicates grid cells where the difference to the Last Millennium values is not significant according to a Welch's t-test ($\alpha > 0.01$).

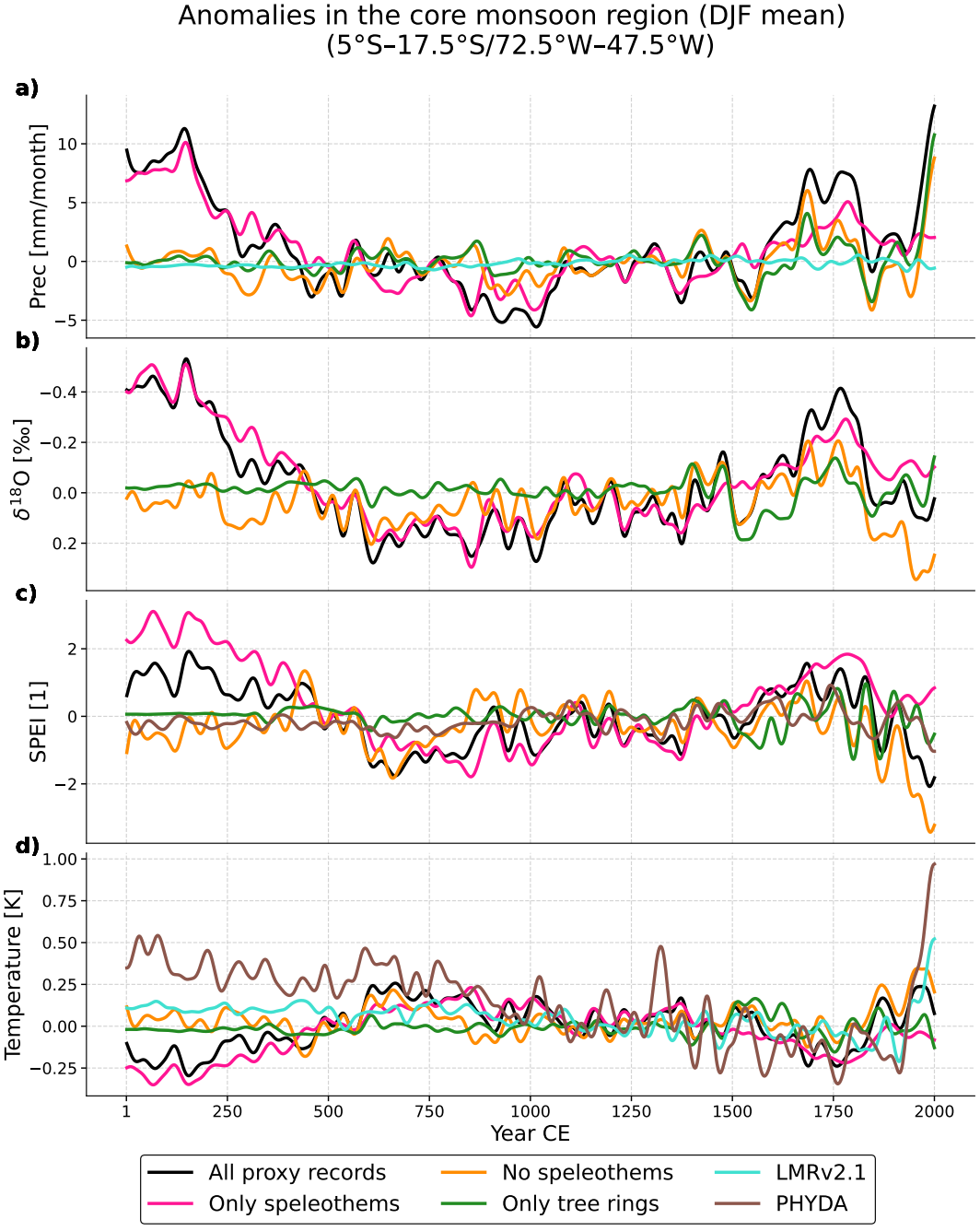

Figure S4.5. Same as Figure 4 for the austral summer (DJF) reconstruction with extended y-axes ranges. The PHYDA reconstruction displayed here is a specific austral summer reconstruction, whereas LMRv2.1 is only provided at an annual time scale.

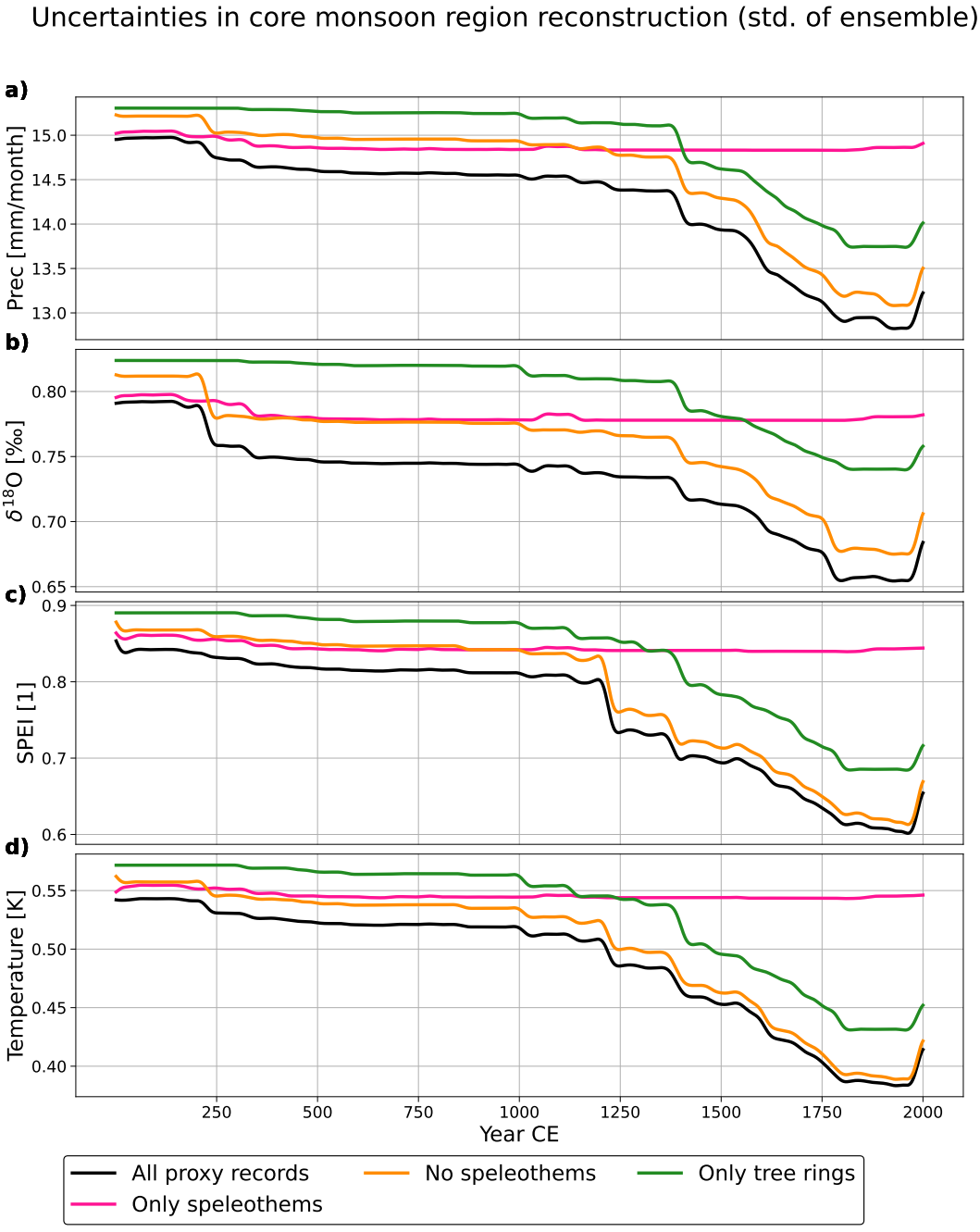

Figure S4.6. Reconstruction uncertainty for the indices from Figure 4 defined as the standard deviation of the posterior ensemble. Here, we display the mean of the standard deviations of the five single model reconstructions, although also other multi-model ensemble error definitions in terms of the propagation of uncertainty are conceivable.

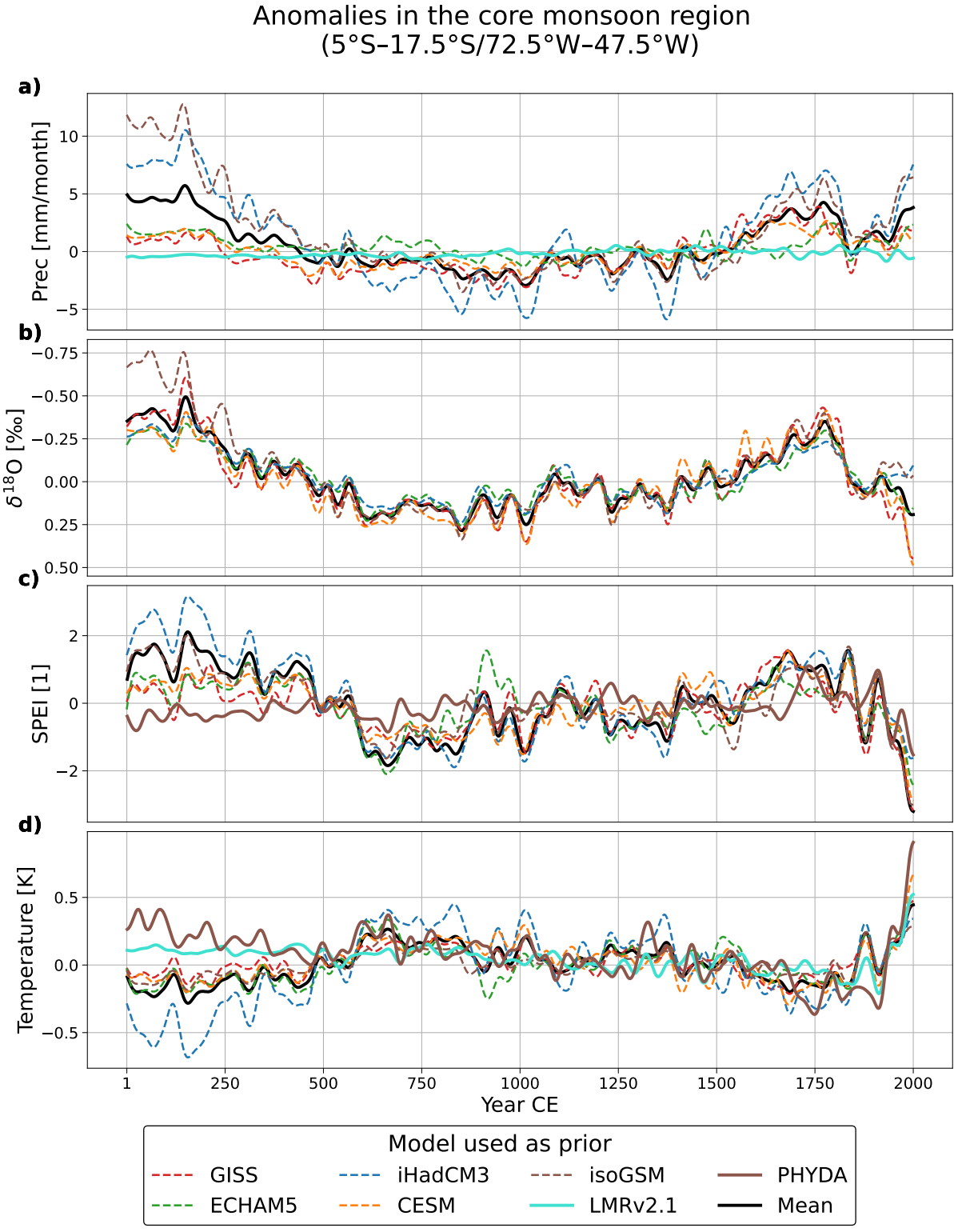

Figure S4.7. Same as Figure 4 including the single model reconstructions using all proxy records (dotted lines). The black line is the multi-model ensemble reconstruction (mean of single prior reconstructions).

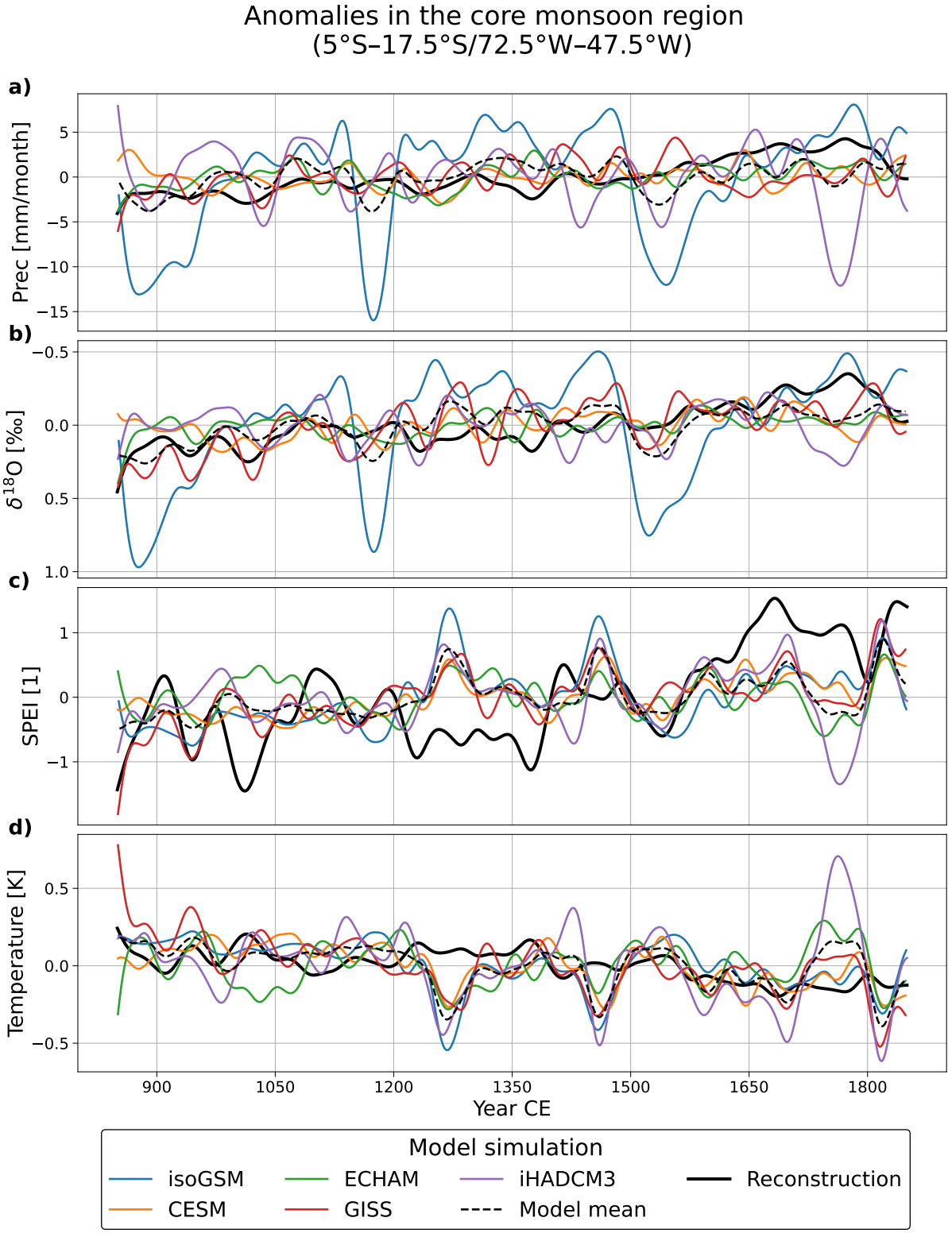

Figure S4.8. Same as Figure 4 for the *all proxies* reconstruction and the model simulations. The time period has been limited to the period 850-1850 CE as this is the time span covered by the model simulations.

Additional power spectra

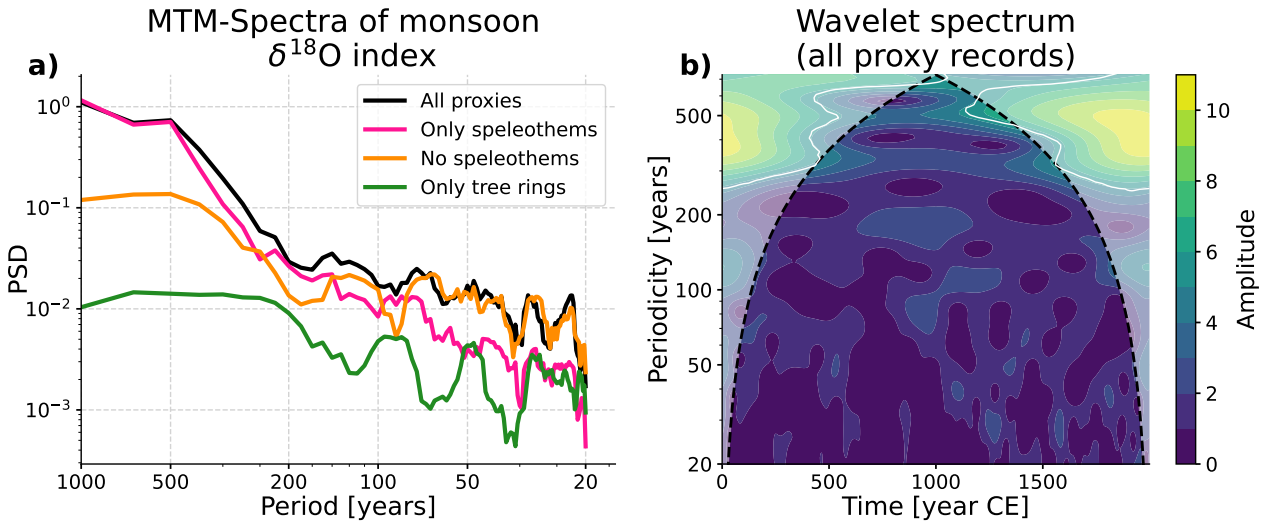

Figure S4.9. Spectra of reconstructed monsoon δ^{18}O index. See description of Figure 6.

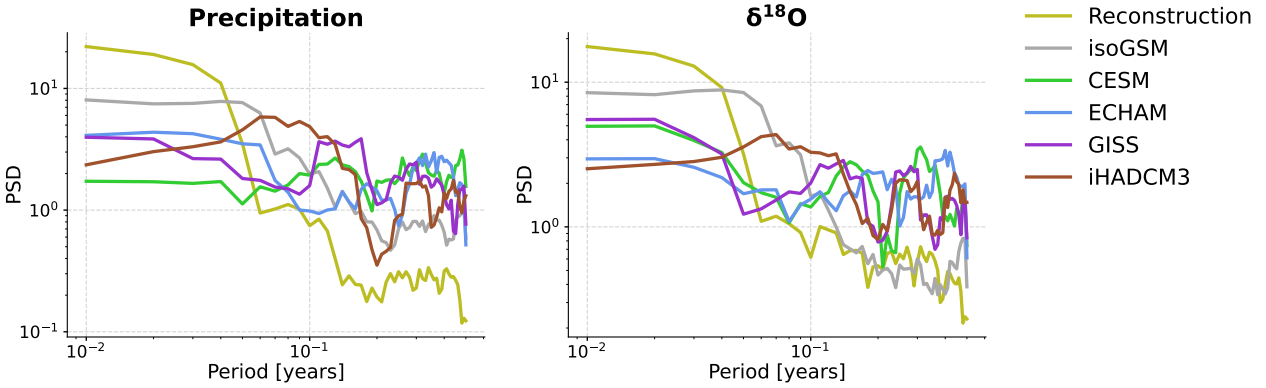

Figure S4.10. Spectra of SASM indices in model simulations. The spectra for SASM precipitation and δ^{18}O have been computed as in Figure 6, but limited to the period 850-1850 CE, because this is the time period covered by the model simulations. In addition, all time series have been standardized, as the model simulations have more overall variability (higher variance). Standardizing the time series allows to highlight the different scaling of the simulation and reconstruction spectra.

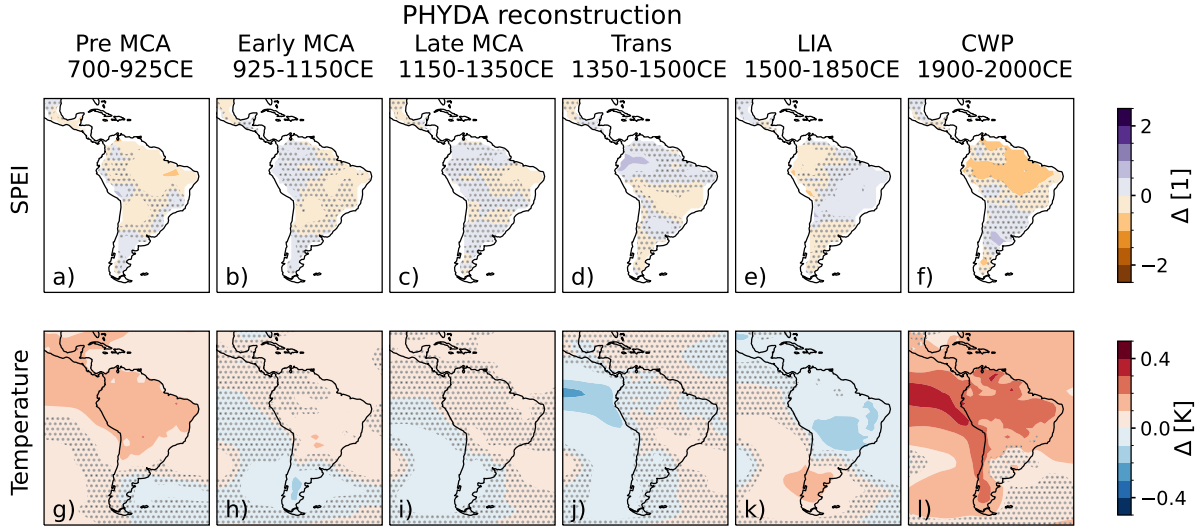

Figure S4.11. Same Anomaly Fields as Figure 3 for the PHYDA reconstruction (Steiger et al., 2018), which includes temperature and SPEI among its reconstructed variables, but not precipitation and δ^{18}O. Stippling indicates grid cells where the difference to the Last Millennium values is not significant according to a Welch's t-test ($\alpha > 0.01$).

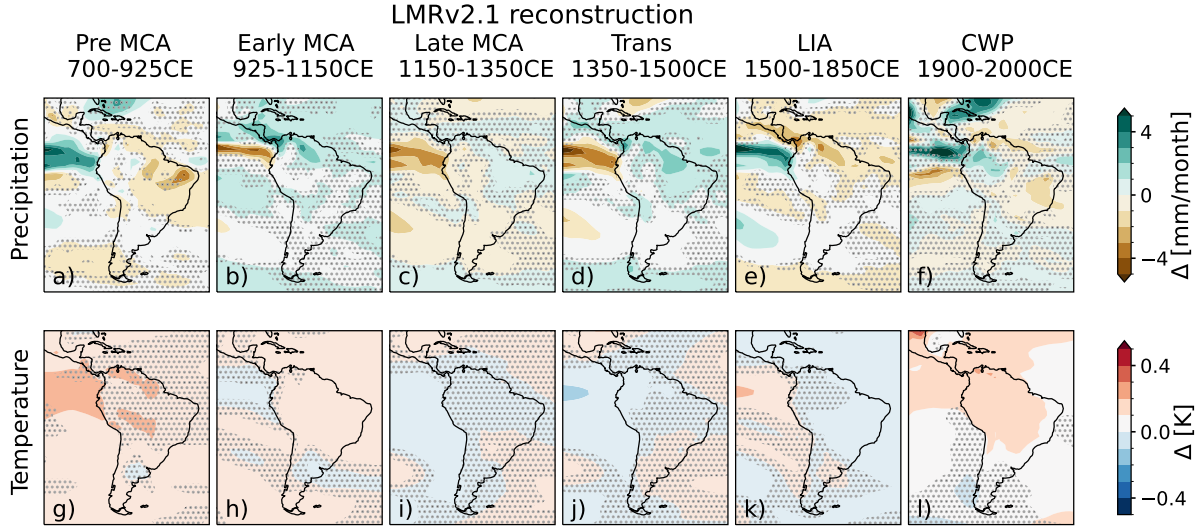

Figure S4.12. Same Anomaly Fields as Figure 3 for the LMRv2.1 reconstruction (Tardif et al., 2019), which includes temperature and precipitation among its reconstructed variables, but not SPEI and δ^{18}O. Stippling indicates grid cells where the difference to the Last Millennium values is not significant according to a Welch's t-test ($\alpha > 0.01$).

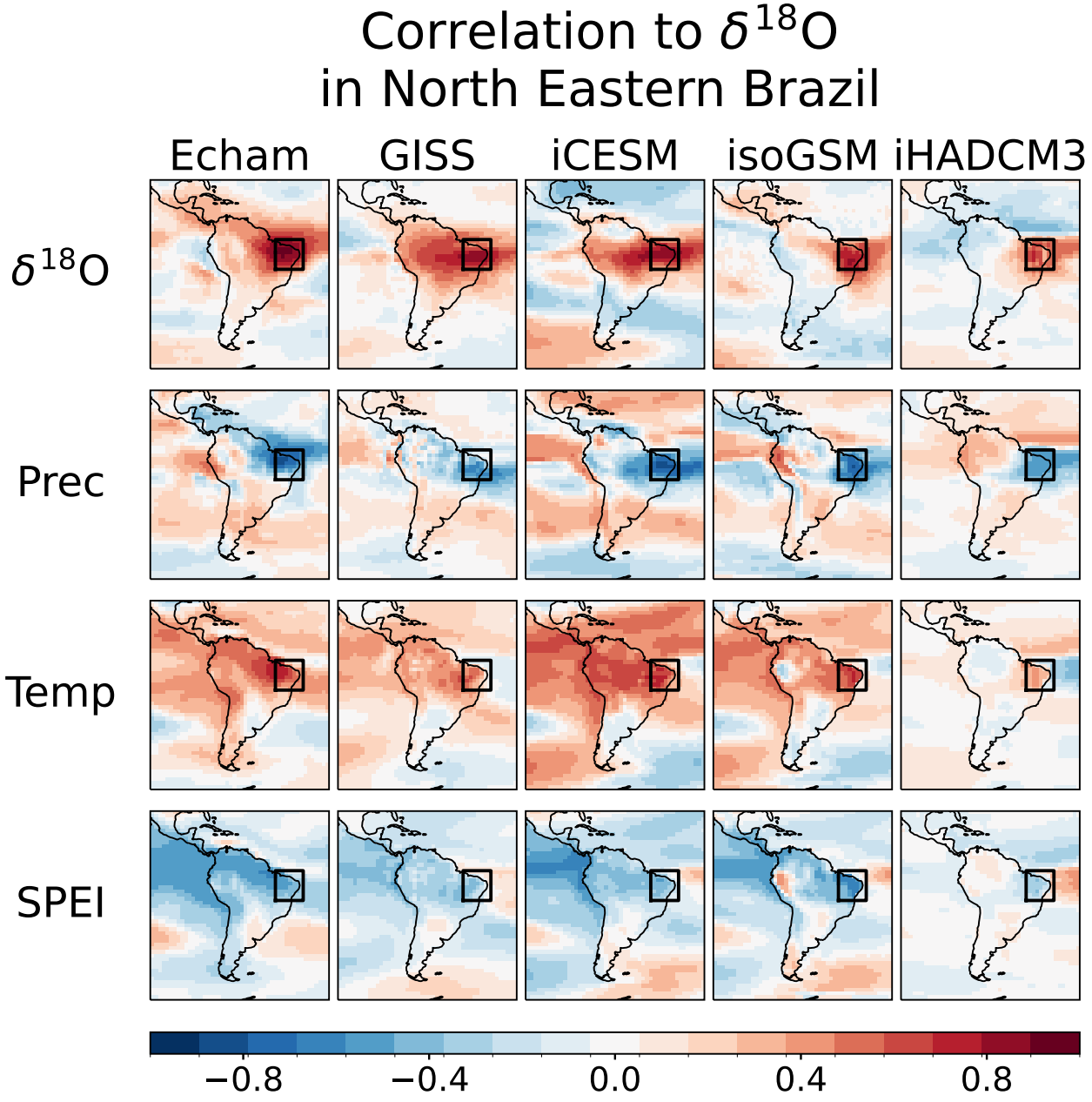

Figure S4.13. Correlation of δ^{18}O mean in the Nordeste (black box, Lat: -15-0°, Lon: 313-327°) to climate variables δ^{18}O, precipitation, temperature and SPEI of individual grid cells in the five isotope-enabled climate model simulations. The correlations have been computed with the annual mean values of the simulated climate variables.

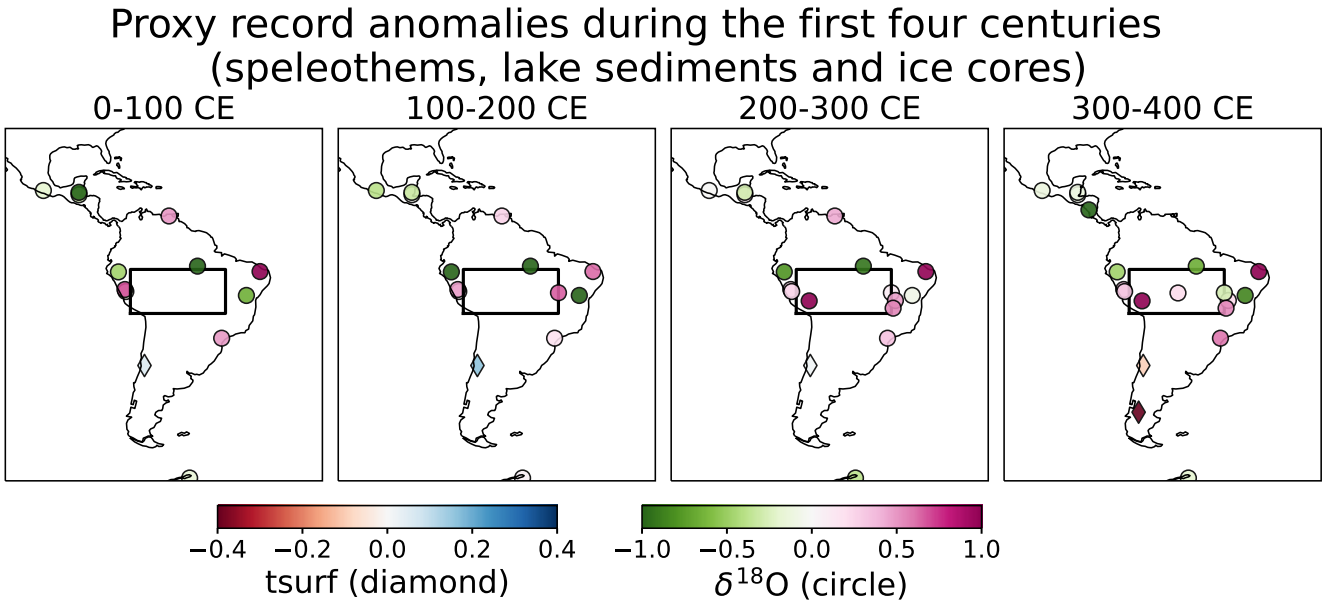

Figure S4.14. Proxy record anomalies during the first four centuries of the CE with respect to the Last Millennium mean.

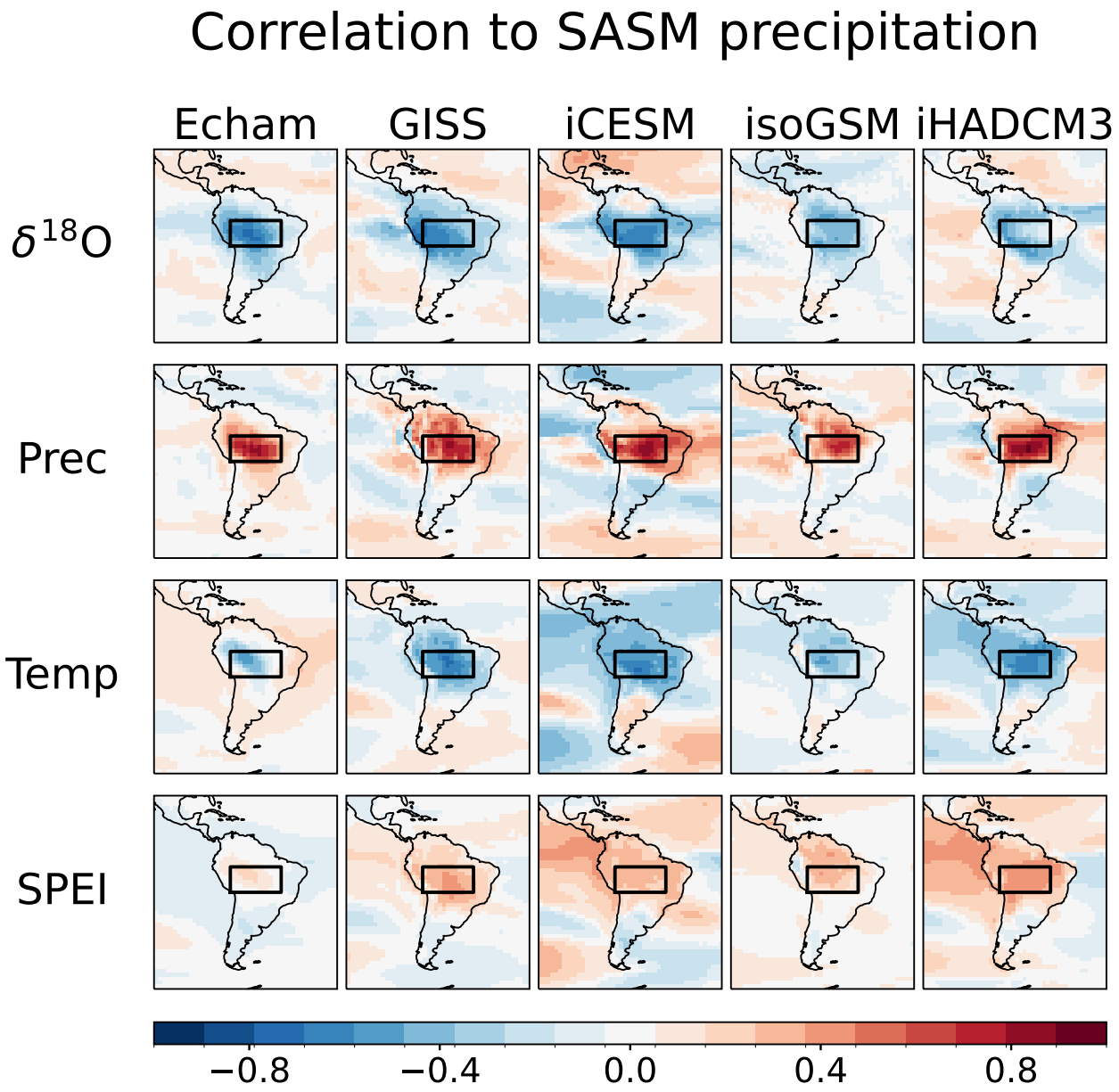

Figure S4.15. Correlation of precipitation mean in core SASM region (black box, Lat: -17.5 - -5°, Lon: 287.5-312.5°) to climate variables δ^{18}O, precipitation, temperature and SPEI of individual grid cells in the five isotope-enabled climate model simulations. The correlations have been computed with the annual mean values of the simulated climate variables.

References

Abram, N. J., Mulvaney, R., Wolff, E. W., Triest, J., Kipfstuhl, S., Trusel, L. D., Vimeux, F., Fleet, L., and Arrowsmith, C.: Acceleration of snow melt in an Antarctic Peninsula ice core during the twentieth century, Nature Geoscience, 6, 404–411, https://doi.org/10.1038/ngeo1787, 2013.

Akers, P. D., Brook, G. A., Railsback, L. B., Liang, F., Iannone, G., Webster, J. W., Reeder, P. P., Cheng, H., and Edwards, R. L.: An extended and higher-resolution record of climate and land use from stalagmite MC01 from Macal Chasm, Belize, revealing connections between major dry events, overall climate variability, and Maya sociopolitical changes, Palaeogeography, Palaeoclimatology, Palaeoecology, 459, 268–288, https://doi.org/10.1016/j.palaeo.2016.07.007, 2016.

Apaéstegui, J., Cruz, F. W., Sifeddine, A., Vuille, M., Espinoza, J. C., Guyot, J. L., Khodri, M., Strikis, N., Santos, R. V., Cheng, H., Edwards, L., Carvalho, E., and Santini, W.: Hydroclimate Variability of the Northwestern Amazon Basin near the Andean Foothills of Peru Related to the South American Monsoon System during the Last 1600 Years, Climate of the Past, 10, 1967–1981, https://doi.org/10.5194/cp-10-1967-2014, 2014.

Apaéstegui, J., Cruz, F. W., Vuille, M., Fohlmeister, J., Espinoza, J. C., Sifeddine, A., Strikis, N., Guyot, J. L., Ventura, R., Cheng, H., and Edwards, R. L.: Precipitation Changes over the Eastern Bolivian Andes Inferred from Speleothem (δ18O) Records for the Last 1400 Years, Earth and Planetary Science Letters, 494, 124–134, https://doi.org/10.1016/j.epsl.2018.04.048, 2018.

Azevedo, V., Stríkis, N. M., Santos, R. A., de Souza, J. G., Ampuero, A., Cruz, F. W., de Oliveira, P., Iriarte, J., Stumpf, C. F., Vuille, M., Mendes, V. R., Cheng, H., and Edwards, R. L.: Medieval Climate Variability in the Eastern Amazon-Cerrado Regions and Its Archeological Implications, Scientific Reports, 9, 20 306, https://doi.org/10.1038/s41598-019-56852-7, 2019.

Bird, B. W., Abbott, M. B., Rodbell, D. T., and Vuille, M.: Holocene Tropical South American Hydroclimate Revealed from a Decadally Resolved Lake Sediment δ18O Record, Earth and Planetary Science Letters, 310, 192–202, https://doi.org/10.1016/j.epsl.2011.08.040, 2011a.

Bird, B. W., Abbott, M. B., Vuille, M., Rodbell, D. T., Stansell, N. D., and Rosenmeier, M. F.: A 2,300-Year-Long Annually Resolved Record of the South American Summer Monsoon from the Peruvian Andes, Proceedings of the National Academy of Sciences, 108, 8583–8588, https://doi.org/10.1073/pnas.1003719108, 2011b.

Black, D. E., Abahazi, M. A., Thunell, R. C., Kaplan, A., Tappa, E. J., and Peterson, L. C.: An 8-Century Tropical Atlantic SST Record from the Cariaco Basin: Baseline Variability, Twentieth-Century Warming, and Atlantic Hurricane Frequency, Paleoceanography, 22, https://doi.org/10.1029/2007PA001427, 2007.

Boës, X. and Fagel, N.: Relationships between Southern Chilean Varved Lake Sediments, Precipitation and ENSO for the Last 600 Years, Journal of Paleolimnology, 39, 237–252, https://doi.org/10.1007/s10933-007-9119-9, 2008.

Breitenmoser, P., Brönnimann, S., and Frank, D.: Forward Modelling of Tree-Ring Width and Comparison with a Global Network of Tree-Ring Chronologies, Climate of the Past, 10, 437–449, https://doi.org/10.5194/cp-10-437-2014, 2014.

Bretherton, C. S., Widmann, M., Dymnikov, V. P., Wallace, J. M., and Bladé, I.: The Effective Number of Spatial Degrees of Freedom of a Time-Varying Field, Journal of Climate, 12, 1990–2009, https://doi.org/10.1175/1520-0442(1999)012<1990:TENOSD>2.0.CO;2, 1999.

Bustamante, M., Cruz, F., Vuille, M., Apaéstegui, J., Strikis, N., Panizo, G., Novello, F., Deininger, M., Sifeddine, A., Cheng, H., Moquet, J., Guyot, J., Santos, R., Segura, H., and Edwards, R.: Holocene changes in monsoon precipitation in the Andes of NE Peru based on δ 18O speleothem records, Quaternary Science Reviews, 146, 274–287, https://doi.org/10.1016/j.quascirev.2016.05.023, 2016.

Compo, G. P., Whitaker, J. S., Sardeshmukh, P. D., Matsui, N., Allan, R. J., Yin, X., Gleason, B. E., Vose, R. S., Rutledge, G., Bessemoulin, P., Brönnimann, S., Brunet, M., Crouthamel, R. I., Grant, A. N., Groisman, P. Y., Jones, P. D., Kruk, M. C., Kruger, A. C., Marshall, G. J., Maugeri, M., Mok, H. Y., Nordli, Ø., Ross, T. F., Trigo, R. M., Wang, X. L., Woodruff, S. D., and Worley, S. J.: The Twentieth Century Reanalysis Project, Quarterly Journal of the Royal Meteorological Society, 137, 1–28, https://doi.org/10.1002/qj.776, 2011.

de Jong, R., von Gunten, L., Maldonado, A., and Grosjean, M.: Late Holocene Summer Temperatures in the Central Andes Reconstructed from the Sediments of High-Elevation Laguna Chepical, Chile (32° S), Climate of the Past, 9, 1921–1932, https://doi.org/10.5194/cp-9-1921-2013, 2013.

DeLong, K. L., Flannery, J. A., Poore, R. Z., Quinn, T. M., Maupin, C. R., Lin, K., and Shen, C.-C.: A reconstruction of sea surface temperature variability in the southeastern Gulf of Mexico from 1734 to 2008 CE using cross-dated Sr/Ca records from the coral Siderastrea siderea, Paleoceanography, 29, 403–422, 2014.

Dunbar, R. B., Wellington, G. M., Colgan, M. W., and Glynn, P. W.: Eastern Pacific sea surface temperature since 1600 AD: The δ18O record of climate variability in Galápagos corals, Paleoceanography, 9, 291–315, 1994.

Elbert, J., Wartenburger, R., von Gunten, L., Urrutia, R., Fischer, D., Fujak, M., Hamann, Y., Greber, N. D., and Grosjean, M.: Late Holocene air temperature variability reconstructed from the sediments of Laguna Escondida, Patagonia, Chile (45°30′S), Palaeogeography, Palaeoclimatology, Palaeoecology, 369, 482–492, https://doi.org/10.1016/j.palaeo.2012.11.013, 2013.

Elbert, J., Jacques-Coper, M., Van Daele, M., Urrutia, R., and Grosjean, M.: A 600 Years Warm-Season Temperature Record from Varved Sediments of Lago Plomo, Northern Patagonia, Chile (47°S), Quaternary International, 377, 28–37, https://doi.org/10.1016/j.quaint.2015.01.004, 2015.

Emile-Geay, J., McKay, N. P., Kaufman, D. S., von Gunten, L., Wang, J., Anchukaitis, K. J., Abram, N. J., Addison, J. A., Curran, M. A., Evans, M. N., Henley, B. J., Hao, Z., Martrat, B., McGregor, H. V., Neukom, R., Pederson, G. T., Stenni, B., Thirumalai, K., Werner, J. P., Xu, C., Divine, D. V., Dixon, B. C., Gergis, J., Mundo, I. A., Nakatsuka, T., Phipps, S. J., Routson, C. C., Steig, E. J., Tierney, J. E., Tyler, J. J., Allen, K. J., Bertler, N. A., Björklund, J., Chase, B. M., Chen, M.-T., Cook, E., de Jong, R., DeLong, K. L., Dixon, D. A., Ekaykin, A. A., Ersek, V., Filipsson, H. L., Francus, P., Freund, M. B., Frezzotti, M., Gaire, N. P., Gajewski, K., Ge, Q., Goosse, H., Gornostaeva, A., Grosjean, M., Horiuchi, K., Hormes, A., Husum, K., Isaksson, E., Kandasamy, S., Kawamura, K., Kilbourne, K. H., Koç, N., Leduc, G., Linderholm, H. W., Lorrey, A. M., Mikhalenko, V., Mortyn, P. G., Motoyama, H., Moy, A. D., Mulvaney, R., Munz, P. M., Nash, D. J., Oerter, H., Opel, T., Orsi, A. J., Ovchinnikov, D. V., Porter, T. J., Roop, H. A., Saenger, C., Sano, M., Sauchyn, D., Saunders, K. M., Seidenkrantz, M.-S., Severi, M., Shao, X., Sicre, M.-A., Sigl, M., Sinclair, K., St. George, S., St. Jacques, J.-M., Thamban, M., Kuwar Thapa, U., Thomas, E. R., Turney, C., Uemura, R., Viau, A. E., Vladimirova, D. O., Wahl, E. R., White, J. W., Yu, Z., Zinke, J., and PAGES2k Consortium: A Global Multiproxy Database for Temperature Reconstructions of the Common Era, Scientific Data, 4, 170 088, https://doi.org/10.1038/sdata.2017.88, 2017.

Fensterer, C., Scholz, D., Hoffmann, D., Spötl, C., Pajón, J. M., and Mangini, A.: Cuban stalagmite suggests relationship between Caribbean precipitation and the Atlantic Multidecadal Oscillation during the past 1.3 ka, The Holocene, 22, 1405–1412, https://doi.org/10.1177/0959683612449759, 2012.

Garreaud, R. D., Vuille, M., Compagnucci, R., and Marengo, J.: Present-Day South American Climate, Palaeogeography, Palaeoclimatology, Palaeoecology, 281, 180–195, https://doi.org/10.1016/j.palaeo.2007.10.032, 2009.

Gneiting, T. and Raftery, A. E.: Strictly Proper Scoring Rules, Prediction, and Estimation, Journal of the American Statistical Association, 102, 359–378, https://doi.org/10.1198/016214506000001437, 2007.

Grießinger, J., Langhamer, L., Schneider, C., Saß, B.-L., Steger, D., Skvarca, P., Braun, M. H., Meier, W. J.-H., Srur, A. M., and Hochreuther, P.: Imprints of Climate Signals in a 204 Year δ18O Tree-Ring Record of Nothofagus Pumilio From Perito Moreno Glacier, Southern Patagonia (50°S), Frontiers in Earth Science, 6, 2018.

Haase-Schramm, A., Böhm, F., Eisenhauer, A., Dullo, W.-C., Joachimski, M. M., Hansen, B., and Reitner, J.: Sr/Ca Ratios and Oxygen Isotopes from Sclerosponges: Temperature History of the Caribbean Mixed Layer and Thermocline during the Little Ice Age: SR/CA AND δ^{18} O FROM SCLEROSPONGES, Paleoceanography, 18, n/a–n/a, https://doi.org/10.1029/2002PA000830, 2003.

Harris, I., Osborn, T. J., Jones, P., and Lister, D.: Version 4 of the CRU TS monthly high-resolution gridded multivariate climate dataset, Scientific Data, 7, https://doi.org/10.1038/s41597-020-0453-3, 2020.

Hoffmann, G., Ramirez, E., Taupin, J. D., Francou, B., Ribstein, P., Delmas, R., Dürr, H., Gallaire, R., Simões, J., Schotterer, U., Stievenard, M., and Werner, M.: Coherent Isotope History of Andean Ice Cores over the Last Century, Geophysical Research Letters, 30, https://doi.org/10.1029/2002GL014870, 2003.

Humanes-Fuente, V., Ferrero, M. E., Muñoz, A. A., González-Reyes, Á., Requena-Rojas, E. J., Barichivich, J., Inga, J. G., and Layme-Huaman, E. T.: Two Centuries of Hydroclimatic Variability Reconstructed From Tree-Ring Records Over the Amazonian Andes of Peru, Journal of Geophysical Research: Atmospheres, 125, e2020JD032 565, https://doi.org/10.1029/2020JD032565, 2020.

Kanner, L. C., Burns, S. J., Cheng, H., Edwards, R. L., and Vuille, M.: High-resolution variability of the South American summer monsoon over the last seven millennia: insights from a speleothem record from the central Peruvian Andes, Quaternary Science Reviews, 75, 1–10, https://doi.org/10.1016/j.quascirev.2013.05.008, 2013.

Kennett, D. J., Breitenbach, S. F. M., Aquino, V. V., Asmerom, Y., Awe, J., Baldini, J. U., Bartlein, P., Culleton, B. J., Ebert, C., Jazwa, C., Macri, M. J., Marwan, N., Polyak, V., Prufer, K. M., Ridley, H. E., Sodemann, H., Winterhalder, B., and Haug, G. H.: Development and Disintegration of Maya Political Systems in Response to Climate Change, Science, 338, 788–791, https://doi.org/10.1126/science.1226299, 2012.

Kilbourne, K., Quinn, T., Webb, R., Guilderson, T., Nyberg, J., and Winter, A.: Paleoclimate proxy perspective on Caribbean climate since the year 1751: Evidence of cooler temperatures and multidecadal variability, Paleoceanography, 23, 2008.

Konecky, B. L., McKay, N. P., Churakova (Sidorova), O. V., Comas-Bru, L., Dassié, E. P., DeLong, K. L., Falster, G. M., Fischer, M. J., Jones, M. D., Jonkers, L., Kaufman, D. S., Leduc, G., Managave, S. R., Martrat, B., Opel, T., Orsi, A. J., Partin, J. W., Sayani, H. R., Thomas, E. K., Thompson, D. M., Tyler, J. J., Abram, N. J., Atwood, A. R., Cartapanis, O., Conroy, J. L., Curran, M. A., Dee, S. G., Deininger, M., Divine, D. V., Kern, Z., Porter, T. J., Stevenson, S. L., von Gunten, L., and Members, I. P.: The Iso2k Database: A Global Compilation of Paleo-δ^{18}O and δ^{2}H Records to Aid Understanding of Common Era Climate, Earth System Science Data, 12, 2261–2288, https://doi.org/10.5194/essd-12-2261-2020, 2020.

Lachniet, M. S., Bernal, J. P., Asmerom, Y., Polyak, V., and Piperno, D.: A 2400 yr Mesoamerican rainfall reconstruction links climate and cultural change, Geology, 40, 259–262, https://doi.org/10.1130/g32471.1, 2012.

Libera, M. E. D., Novello, V. F., Cruz, F. W., Orrison, R., Vuille, M., Maezumi, S. Y., de Souza, J., Cauhy, J., Campos, J. L. P. S., Ampuero, A., Utida, G., Stríkis, N. M., Stumpf, C. F., Azevedo, V., Zhang, H., Edwards, R. L., and Cheng, H.: Paleoclimatic and paleoenvironmental changes in Amazonian lowlands over the last three millennia, Quaternary Science Reviews, 279, 107 383, https://doi.org/10.1016/j.quascirev.2022.107383, 2022.

Linsley, B. K., Dunbar, R. B., Wellington, G. M., and Mucciarone, D. A.: A coral-based reconstruction of Intertropical Convergence Zone variability over Central America since 1707, Journal of Geophysical Research: Oceans, 99, 9977–9994, 1994.

Medina, N. M. M., Cruz, F. W., Winter, A., Zhang, H., Ampuero, A., Vuille, M., Mayta, V. C., Campos, M. C., Rámirez, V. M., Utida, G., Zúñiga, A. C., and Cheng, H.: Atlantic ITCZ variability during the Holocene based on high-resolution speleothem isotope records from northern Venezuela, Quaternary Science Reviews, 307, 108 056, https://doi.org/https://doi.org/10.1016/j.quascirev.2023.108056, 2023.

Medina-Elizalde, M., Burns, S. J., Lea, D. W., Asmerom, Y., von Gunten, L., Polyak, V., Vuille, M., and Karmalkar, A.: High resolution stalagmite climate record from the Yucatán Peninsula spanning the Maya terminal classic period, Earth and Planetary Science Letters, 298, 255–262, https://doi.org/10.1016/j.epsl.2010.08.016, 2010.

Morales, M. S., Christie, D. A., Villalba, R., Argollo, J., Pacajes, J., Silva, J. S., Alvarez, C. A., Llancabure, J. C., and Soliz Gamboa, C. C.: Precipitation Changes in the South American Altiplano since 1300 AD Reconstructed by Tree-Rings, Climate of the Past, 8, 653–666, https://doi.org/10.5194/cp-8-653-2012, 2012.

Morales, M. S., Cook, E. R., Barichivich, J., Christie, D. A., Villalba, R., LeQuesne, C., Srur, A. M., Ferrero, M. E., González-Reyes, Á., Couvreux, F., et al.: Six hundred years of South American tree rings reveal an increase in severe hydroclimatic events since mid-20th century, Proceedings of the National Academy of Sciences, 117, 16 816–16 823, 2020.

Morales, M. S., Crispín-DelaCruz, D. B., Álvarez, C., Christie, D. A., Ferrero, M. E., Andreu-Hayles, L., Villalba, R., Guerra, A., Ticse-Otarola, G., Rodríguez-Ramírez, E. C., LLocclla-Martínez, R., Sanchez-Ferrer, J., and Requena-Rojas, E. J.: Drought Increase since the Mid-20th Century in the Northern South American Altiplano Revealed by a 389-Year Precipitation Record, Climate of the Past, 19, 457–476, https://doi.org/10.5194/cp-19-457-2023, 2023.

Neukom, R. and Gergis, J.: Southern Hemisphere High-Resolution Palaeoclimate Records of the Last 2000 Years, The Holocene, 22, 501–524, https://doi.org/10.1177/0959683611427335, 2012.

Neukom, R., del Rosario Prieto, M., Moyano, R., Luterbacher, J., Pfister, C., Villalba, R., Jones, P. D., and Wanner, H.: An Extended Network of Documentary Data from South America and Its Potential for Quantitative Precipitation Reconstructions Back to the 16th Century, Geophysical Research Letters, 36, L12 703, https://doi.org/10.1029/2009GL038351, 2009.

Neukom, R., Luterbacher, J., Villalba, R., Küttel, M., Frank, D., Jones, P. D., Grosjean, M., Esper, J., Lopez, L., and Wanner, H.: Multi-Centennial Summer and Winter Precipitation Variability in Southern South America, Geophysical Research Letters, 37, https://doi.org/10.1029/2010GL043680, 2010.

Neukom, R., Luterbacher, J., Villalba, R., Küttel, M., Frank, D., Jones, P. D., Grosjean, M., Wanner, H., Aravena, J.-C., Black, D. E., et al.: Multiproxy summer and winter surface air temperature field reconstructions for southern South America covering the past centuries, Climate Dynamics, 37, 35–51, 2011.

Novello, V. F., Cruz, F. W., Karmann, I., Burns, S. J., Stríkis, N. M., Vuille, M., Cheng, H., Lawrence Edwards, R., Santos, R. V., Frigo, E., and Barreto, E. A. S.: Multidecadal Climate Variability in Brazil's Nordeste during the Last 3000 Years Based on Speleothem Isotope Records, Geophysical Research Letters, 39, https://doi.org/10.1029/2012GL053936, 2012.

Novello, V. F., Vuille, M., Cruz, F. W., Stríkis, N. M., de Paula, M. S., Edwards, R. L., Cheng, H., Karmann, I., Jaqueto, P. F., Trindade, R. I. F., Hartmann, G. A., and Moquet, J. S.: Centennial-Scale Solar Forcing of the South American Monsoon System Recorded in Stalagmites, Scientific Reports, 6, 24 762, https://doi.org/10.1038/srep24762, 2016.

Novello, V. F., Cruz, F. W., Moquet, J. S., Vuille, M., de Paula, M. S., Nunes, D., Edwards, R. L., Cheng, H., Karmann, I., Utida, G., Stríkis, N. M., and Campos, J. L. P. S.: Two Millennia of South Atlantic Convergence Zone Variability Reconstructed From Isotopic Proxies, Geophysical Research Letters, 45, 5045–5051, https://doi.org/10.1029/2017GL076838, 2018.

Novello, V. F., William da Cruz, F., Vuille, M., Pereira Silveira Campos, J. L., Stríkis, N. M., Apaéstegui, J., Moquet, J. S., Azevedo, V., Ampuero, A., Utida, G., Wang, X., Paula-Santos, G. M., Jaqueto, P., Ruiz Pessenda, L. C., Breecker, D. O., and Karmann, I.: Investigating δ13C Values in Stalagmites from Tropical South America for the Last Two Millennia, Quaternary Science Reviews, 255, 106 822, https://doi.org/10.1016/j.quascirev.2021.106822, 2021.

Rohde, R. A. and Hausfather, Z.: The Berkeley Earth Land/Ocean Temperature Record, Earth System Science Data, 12, 3469–3479, https://doi.org/10.5194/essd-12-3469-2020, 2020.

Saenger, C., Cohen, A. L., Oppo, D. W., Halley, R. B., and Carilli, J. E.: Surface-Temperature Trends and Variability in the Low-Latitude North Atlantic since 1552, Nature Geoscience, 2, 492–495, https://doi.org/10.1038/ngeo552, 2009.

Schneider, U., Fuchs, T., Meyer-Christoffer, A., and Rudolf, B.: Global precipitation analysis products of the GPCC, Global Precipitation Climatology Centre (GPCC), DWD, Internet Publikation, 112, 2008.

Stansell, N. D., Steinman, B. A., Abbott, M. B., Rubinov, M., and Roman-Lacayo, M.: Lacustrine Stable Isotope Record of Precipitation Changes in Nicaragua during the Little Ice Age and Medieval Climate Anomaly, Geology, 41, 151–154, https://doi.org/10.1130/G33736.1, 2013.

Steiger, N. J., Hakim, G. J., Steig, E. J., Battisti, D. S., and Roe, G. H.: Assimilation of Time-Averaged Pseudoproxies for Climate Reconstruction, Journal of Climate, 27, 426–441, https://doi.org/10.1175/JCLI-D-12-00693.1, 2014.

Steiger, N. J., Smerdon, J. E., Cook, E. R., and Cook, B. I.: A Reconstruction of Global Hydroclimate and Dynamical Variables over the Common Era, Scientific Data, 5, 180 086, https://doi.org/10.1038/sdata.2018.86, 2018.

Swart, P. K., Dodge, R. E., and Hudson, H. J.: A 240-year stable oxygen and carbon isotopic record in a coral from South Florida: Implications for the prediction of precipitation in southern Florida, Palaios, pp. 362–375, 1996.

Tardif, R., Hakim, G. J., Perkins, W. A., Horlick, K. A., Erb, M. P., Emile-Geay, J., Anderson, D. M., Steig, E. J., and Noone, D.: Last Millennium Reanalysis with an Expanded Proxy Database and Seasonal Proxy Modeling, Climate of the Past, 15, 1251–1273, https://doi.org/10.5194/cp-15-1251-2019, 2019.

Thompson, L. G., Mosley-Thompson, E., Davis, M. E., Zagorodnov, V. S., Howat, I. M., Mikhalenko, V. N., and Lin, P.-N.: Annually Resolved Ice Core Records of Tropical Climate Variability over the Past ~1800 Years, Science, 340, 945–950, https://doi.org/10.1126/science.1234210, 2013.

Tierney, J. E., Abram, N. J., Anchukaitis, K. J., Evans, M. N., Giry, C., Kilbourne, K. H., Saenger, C. P., Wu, H. C., and Zinke, J.: Tropical sea surface temperatures for the past four centuries reconstructed from coral archives, Paleoceanography, 30, 226–252, https://doi.org/10.1002/2014pa002717, 2015.

Utida, G., Cruz, F. W., Vuille, M., Ampuero, A., Novello, V. F., Maksic, J., Sampaio, G., Cheng, H., Zhang, H., Dias de Andrade, F. R., and Edwards, R. L.: Spatiotemporal ITCZ Dynamics during the Last Three Millennia in Northeastern Brazil and Related Impacts in Modern Human History, Preprint, Proxy Use-Development-Validation/Terrestrial Archives/Holocene, https://doi.org/10.5194/cp-2023-2, 2023.

von Gunten, L., Grosjean, M., Rein, B., Urrutia, R., and Appleby, P.: A quantitative high-resolution summer temperature reconstruction based on sedimentary pigments from Laguna Aculeo, central Chile, back to AD 850, The Holocene, 19, 873–881, https://doi.org/10.1177/0959683609336573, 2009.

Vuille, M., Burns, S. J., Taylor, B. L., Cruz, F. W., Bird, B. W., Abbott, M. B., Kanner, L. C., Cheng, H., and Novello, V. F.: A Review of the South American Monsoon History as Recorded in Stable Isotopic Proxies over the Past Two Millennia, Climate of the Past, 8, 1309–1321, https://doi.org/10.5194/cp-8-1309-2012, 2012.

Wang, X., Edwards, R. L., Auler, A. S., Cheng, H., Kong, X., Wang, Y., Cruz, F. W., Dorale, J. A., and Chiang, H.-W.: Hydroclimate Changes across the Amazon Lowlands over the Past 45,000 Years, Nature, 541, 204–207, https://doi.org/10.1038/nature20787, 2017.

Wilks, D. S.: Forecast verification, in: International geophysics, vol. 100, pp. 301–394, Elsevier, 2011.

Winter, A., Miller, T., Kushnir, Y., Sinha, A., Timmermann, A., Jury, M. R., Gallup, C., Cheng, H., and Edwards, R. L.: Evidence for 800years of North Atlantic multi-decadal variability from a Puerto Rican speleothem, Earth and Planetary Science Letters, 308, 23–28, https://doi.org/10.1016/j.epsl.2011.05.028, 2011.

Wortham, B. E., Wong, C. I., Silva, L. C. R., McGee, D., Montañez, I. P., Troy Rasbury, E., Cooper, K. M., Sharp, W. D., Glessner, J. J. G., and Santos, R. V.: Assessing Response of Local Moisture Conditions in Central Brazil to Variability in Regional Monsoon Intensity Using Speleothem 87Sr/86Sr Values, Earth and Planetary Science Letters, 463, 310–322, https://doi.org/10.1016/j.epsl.2017.01.034, 2017.